JGR Earth Surface

RESEARCH ARTICLE
10.1029/2024JF007817

Dynamic Mud Deposition Along the Fluvial–Tidal Transition Zone in the Waihou River, Aotearoa New Zealand

A. D. La Croix[1], B. Roche[1,2], and J. C. Mullarney[2]

[1]Sedimentary Environments and Analogues Research Group, Earth and Environmental Sciences, School of Science, University of Waikato, Hamilton, New Zealand, [2]Coastal Marine Group, Earth and Environmental Sciences, School of Science, University of Waikato, Hamilton, New Zealand

Key Points:

- Hydrodynamic processes and dynamic mud deposits from a modern system are linked
- Fluid mud and rapidly deposited mud dominate the stratigraphic record, with little mud from gravitational settling
- Dynamic mud conditions may occur throughout the tidal cycle, but cyclic tidal successions are not preserved

Supporting Information:

Supporting Information may be found in the online version of this article.

Correspondence to:

A. D. La Croix,
alacroix@waikato.ac.nz

Citation:

La Croix, A. D., Roche, B., & Mullarney, J. C. (2025). Dynamic mud deposition along the fluvial–tidal transition zone in the Waihou River, Aotearoa New Zealand. *Journal of Geophysical Research: Earth Surface*, *130*, e2024JF007817. https://doi.org/10.1029/2024JF007817

Received 4 MAY 2024
Accepted 24 FEB 2025

Author Contributions:

Conceptualization: A. D. La Croix, J. C. Mullarney
Data curation: A. D. La Croix, B. Roche, J. C. Mullarney
Formal analysis: A. D. La Croix, B. Roche, J. C. Mullarney
Funding acquisition: A. D. La Croix, J. C. Mullarney
Investigation: A. D. La Croix, B. Roche, J. C. Mullarney
Methodology: A. D. La Croix, J. C. Mullarney
Project administration: A. D. La Croix, J. C. Mullarney
Resources: A. D. La Croix, J. C. Mullarney
Software: J. C. Mullarney

Abstract The fluvial–tidal transition zone (FTT) is a critical interface where complex interactions between river flow, tides, and sedimentation shape geomorphic systems and influence the dynamics of aquatic environments. However, few previous studies have integrated real-time hydrodynamic data with sedimentary deposits. In particular, the range of depositional conditions over which mud accumulates remains poorly constrained, and little is understood about how these deposits are preserved in the stratigraphic record. To address this knowledge gap, we examined co-located hydrodynamic instrument data and sedimentary deposits from the lower Waihou River, Aotearoa New Zealand. Results reveal that "dynamic mud" events, including fluid mud and rapidly deposited mud, dominate the spatial and temporal record, with few "static mud" events in which mud is deposited through gravitational settling. We suggest that dynamic mud conditions with the potential for deposition may occur throughout the tidal cycle, although cyclic tidal successions are never fully preserved. Many of the trends in sedimentation observed in studies of larger systems are not present in this small muddy river system, indicating the significance of climatic and river-flow characteristics on the sedimentary record. This work underscores the importance of studying systems of multiple sizes across diverse climatic regimes to establish holistic facies models to reconstruct geological history accurately.

Plain Language Summary In coastal regions where rivers meet the ocean, interactions between river flow, tides, and sediments can shape the environment and influence aquatic ecosystems. However, few studies have monitored both flows and sediment conditions concurrently to allow linking of hydrodynamic processes with sedimentary deposits. As a result, it remains difficult to predict what these environments looked like in the geological past. This study addresses these shortcomings by measuring water flows and sediment loads using oceanographic instrumentation, and comparing these data against sediment cores from the Waihou River on Aotearoa New Zealand's North Island. The results suggest that most mud gets deposited under energetic conditions at several times throughout the tidal cycle. Only rarely does mud seem to sink slowly to the river bottom and get deposited due to gravity-settling. Despite the repetitive rise and fall of tides and river currents, these cyclic processes do not get recorded in the sedimentary deposits. This small muddy river system is quite different from more commonly studied larger systems, as flows exhibit more variability throughout the year. Our research highlights how important it is to study rivers across a range of sizes in different climates to understand how sediment builds up over time and to piece together the depositional history of our planet accurately.

1. Introduction

One of the most complex and dynamic sedimentary environments on Earth lies at the land-sea interface in the fluvial–marine transition of deltas and estuaries. In the channelized portion of the fluvial–marine transition, known as the fluvial–tidal transition zone (FTT), tides modulate river flow, marine water is forced landward, and a mixing zone forms (which is typically accompanied by a turbidity maximum). Hydrodynamics and sedimentation may also be impacted by upstream propagation of tidal bores (Hoitink & Jay, 2016), swell waves impinging on the river mouth (Fagherazzi et al., 2015), convergence of seaward and landward directed sediment transport (Kostaschuk, 2002; Small & Prahl, 2004), and asymmetric circulation driven by river flow, tides, wind, and wind waves (Jay et al., 2015). Additionally, physical (e.g., turbulence), chemical (e.g., salinity), and biological controls on flocculation (e.g., extracellular polymeric substances) can lead to variations in the size of aggregated particles, and hence settling velocities, along tidal rivers (MacDonald & Mullarney, 2015; Maggi, 2009; Sun et al., 2012). The corresponding variations in physical, chemical, and biological conditions, both across and along the FTT,

Supervision: A. D. La Croix, J. C. Mullarney
Visualization: A. D. La Croix
Writing – original draft: A. D. La Croix, B. Roche, J. C. Mullarney
Writing – review & editing: A. D. La Croix, B. Roche, J. C. Mullarney

occur on hourly, daily, and seasonal time scales and manifest in complex sedimentation patterns that are collectively unique to the FTT and the broader fluvial–marine transition (Dalrymple & Choi, 2007).

Although the sedimentary characteristics of the FTT have been investigated extensively in modern systems (Carling et al., 2015; Dalrymple et al., 2003; Dashtgard & La Croix, 2015; Gugliotta et al., 2017; La Croix & Dashtgard, 2015; Nittrouer et al., 2021; Prokocki et al., 2020; Roche, 2022; Smith, 1988) as well in ancient strata (Gugliotta et al., 2016; Jablonski & Dalrymple, 2016; La Croix et al., 2019; Smith, 1987), most studies have focused on characterizing either the hydrodynamic processes operating within the FTT (Jay et al., 2015; Keevil et al., 2015; Wu et al., 2022), or the resulting record of sedimentation (La Croix & Dashtgard, 2015; MacKay & Dalrymple, 2011; Van den Berg et al., 2007). Few studies have attempted to link real-time quantitative measurements of flow parameters to their associated sedimentary deposits. This lack of co-located and synchronous data has resulted in incomplete depositional models for the FTT, which do not fully incorporate the precise process-response linkages.

One major focus of research on the FTT has been the development of generalized depositional models explaining the down-river transition in sedimentary characteristics (which record the time average of sedimentation processes across a range of time scales) from the landward extent of tidal effects into marine-dominated conditions at the seaward extent. Several trends have been identified as useful proxies for determining longitudinal position in the FTT including trends in facies characteristics (Choi et al., 2004; Gugliotta et al., 2017; La Croix & Dashtgard, 2015; Roche, 2022; Van den Berg et al., 2007), stratigraphic architecture (Choi et al., 2021), geomorphology (Dalrymple & Choi, 2007; Gugliotta & Saito, 2019), ichnology (La Croix et al., 2015), sediment geochemistry (Czarnecki et al., 2014; Dashtgard et al., 2022; A. Wang et al., 2021), as well as calcareous microfossils (Armstrong & Brasier, 2005) and palynology (Czarnecki et al., 2014; Dashtgard et al., 2022). One conspicuous feature of deposits that accumulate in the FTT is a general abundance of mud, particularly in depositional positions situated near the time-averaged mixing front of marine and freshwater (i.e., turbidity maximum zone; La Croix & Dashtgard, 2014; van de Lageweg et al., 2018). Traditionally, most mud deposited in the FTT has been interpreted to be the result of gravitational settling during slack water periods (McCave, 1970; Potter et al., 2005), and we refer to these deposits as "static muds." However, mud deposition can occur under a much wider range of conditions, including at fast flow speeds (Baas & Best, 2008; Schieber & Southard, 2009; Schieber et al., 2007) and in completely freshwater (Sutherland et al., 2014); herein, we use the term "dynamic muds" to describe muds that are transported and deposited at flow speeds faster than those at which individual clay grains can settle from the water column.

Using flume experiments, Baas et al. (2009) revealed a predictable progression of flow types arising from increasing suspended sediment concentration (SSC). The study varied the SSC from 0.8 to 434 g L^{-1}, flow velocity from 0.13 to 1.47 m s^{-1}, corresponding to Froude numbers ranging from 0 to ∼1.25 and flow Reynolds numbers from $\sim 10^3$ to $\sim 10^5$. In smaller SSC (less than ∼1 g L^{-1} SSC) flows were fully turbulent (i.e., "turbulent flow"; Baas et al., 2009). Between ∼1 and 10 g L^{-1} SSC turbulence was enhanced near the bed, and flows showed elements of both turbulent and laminar conditions (i.e., "transitional turbulent flow"; Baas et al., 2009). With SSC between ∼10 and 100 g L^{-1} a mobile high-density suspension layer developed below a lutocline and flows could be both turbulent and laminar in the viscous sublayer (i.e., "transitional plug flow"; Baas et al., 2009). Finally, above ∼100 g L^{-1} and up to ∼500 g L^{-1} SSC flows developed laminar shearing under a non-deforming cohesive plug (i.e., "quasi-laminar plug flow"; Baas et al., 2009). When this cohesive plug became stationary on the bed, the flow was referred to as "unstable plug flow" (Baas et al., 2009).

Later, the phase diagrams of Baas et al. (2009) were adopted by MacKay and Dalrymple (2011) to explain that progressive changes in flow regimes can result in the deposition of predictable sets of mud deposits using sedimentary layers from the Cretaceous Bluesky Formation in Alberta, Canada. This previous work has demonstrated that it is theoretically possible for mud to accumulate during any phase of the tidal cycle in FTT channels, although if, and how, deposits differ between different tidal phases and flow conditions is, at present, poorly constrained. Before these longitudinal trends in the abundance and characteristics of mud deposits can be reliably used as a proxy for depositional position, the process-response linkages need to be better elucidated. These knowledge gaps bring about the need to further study modern sedimentary systems to directly link sedimentary processes with depositional response, and to improve depositional models within these complex sedimentary environments.

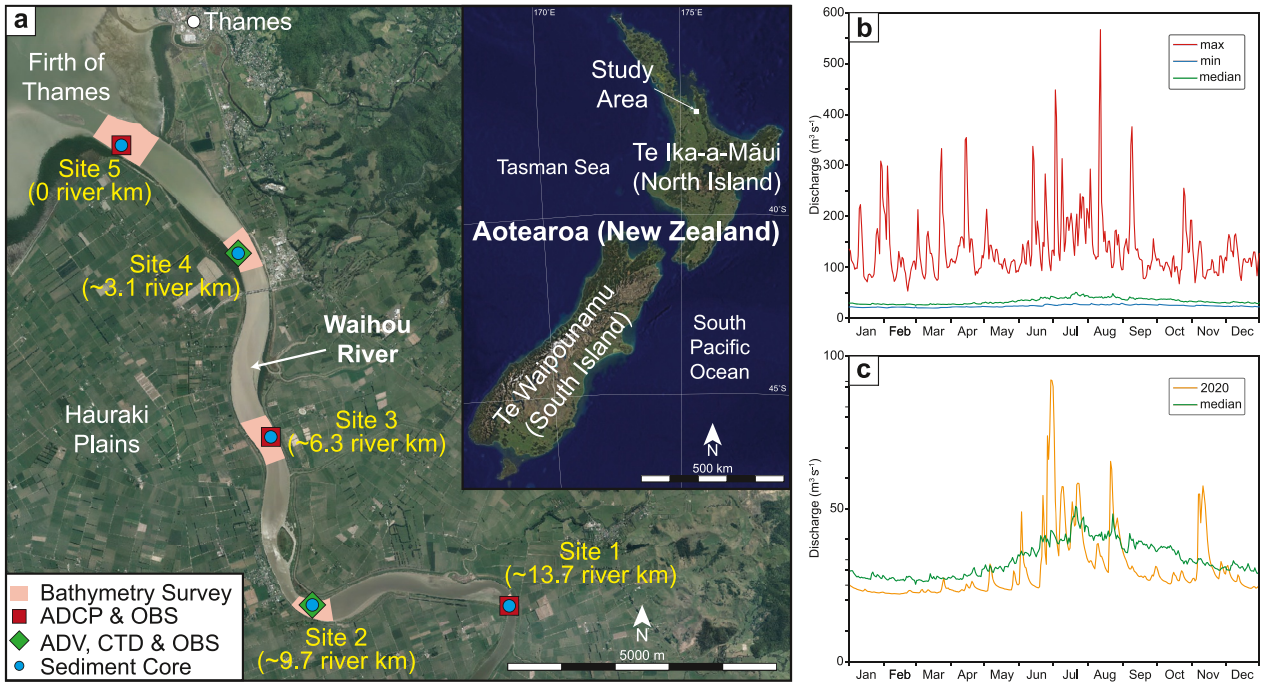

Figure 1. (a) Map showing the Waihou River flowing into the Firth of Thames on Aotearoa New Zealand's North Island. The locations of the five sites where oceanographic and sedimentologic data were collected are labeled. The distance upstream of each site is indicated in river km. (b) Historical mean daily river discharge at Te Aroha from 1962 to 2023. (c) Mean daily discharge for 2020 compared against the historical median (data source: https://waikatoregion.govt.nz, accessed on 12 April 2024).

This study focuses on the coupled hydrodynamic and sedimentary processes operating within an FTT in the Waihou River on New Zealand's North Island. We chose this system as a natural laboratory because of the temperate climatic regime, highly variable flow conditions over short timeframes, and large (for its size) mud-rich sediment load. The study compares a high-resolution record of hydrodynamic processes against co-located and contemporary sedimentary deposits as well as similar deposits that accumulated during the Holocene. Results allow for the identification of different depositional regimes, which vary in both space and time. These data reveal crucial insights into the relationship between flow processes and the corresponding sedimentary signal that encodes these processes, which forms a critical step toward developing more robust depositional models.

2. Study Area

The Waihou River on Aotearoa New Zealand's North Island drains a catchment of 1,984 km^2, and receives 1,450 mm yr^{-1} of precipitation (Figure 1a). The mean annual discharge is 42 m^3 s^{-1}, varying between 20.4 and 566 m^3 s^{-1} (Figure 1b). River flows are broadly seasonal, with low flows <35 m^3 s^{-1} generally occurring in the spring, summer, and early autumn (October–May), whereas high flows are more commonly observed in the late autumn and winter (June–September). However, discharge is flashy, with high flow conditions quickly returning to base flow levels over hours to days (Figures 1b and 1c). The river flows across the Hauraki Plains, the upper portions of which consist of mud, gravel, and pumice of the Late Pleistocene Tauranga Group (Hadfield, 2001). Tributaries of the Waihou River, including the Ohinemuri River (which is the largest), flow from the steep forested mountains of the Kaimai-Coromandel Ranges.

The river debouches into the Firth of Thames, crossing a wide intertidal flat region that is subject to wave influence, which is situated within the back-arc Hauraki Rift (Hochstein & Balance, 1993). Tides at the mouth of the river are semidiurnal and meso-tidal (mean, maximum and minimum tidal ranges are ~2.6, 3.8, and 1.7 m, respectively). The dominant tidal constituents are M2, N2, S2, and K1 with amplitudes of 1.28, 0.26, 0.18, and 0.12 m, respectively. Tidal modulation of river level occurs up to approximately 35 km, and marine water intrudes ~12 km up the channel during high tides (James, 2024; McBride et al., 2016).

The Waihou River system exports approximately 0.16 Mt of sediment each year (Hicks et al., 2011) and is the major source of suspended sediment delivered to the Firth of Thames. The majority of sediment consists of volcanic glass derived from erosion of ignimbrite in the upper catchment (Naish et al., 1993). A large proportion of this material gets retained within the Firth of Thames and is deposited upon the Firth's southern mudflats, mangrove forests (Vundavilli et al., 2021) or along the eastern margins (Pritchard et al., 2015). Owing to the flow characteristics of the Waihou River—which are dictated by the temperate maritime climate (Griffiths & Glasby, 1985; Pritchard et al., 2015)—muddy transport and deposition events are typically short-lived, lasting from a few hours to a few days.

3. Methods

To characterize both the depositional processes and associated characteristics of the sedimentary deposits along the lower Waihou River, several data sets were obtained: bathymetric surveys, time series of hydrodynamic parameters, sediment cores, and surface sediment samples. These data focused on five main study sites, which were equi-spaced along the FTT (Sites 1–5; Figure 1a). Sites were selected to encompass conditions from almost entirely freshwater and tidal to marine. Site 1 ("upstream") is situated ∼13.7 river km upstream from the river mouth (a river km is the distance upstream along the thalweg of the channel). Site 2 is located ∼9.7 river km upstream. Site 3 ("mid-river") is ∼6.3 river km upstream. Site 4 is ∼3.1 river km upstream. Finally, Site 5 ("river mouth") is taken as river km 0.

3.1. Bathymetry

Bathymetric surveys were conducted at each of the five study sites (Figure 1a) using a Lowrance vessel-mounted transducer operating at 200 kHz. Data were collected along three to five across-channel transects and then interpolated to produce bathymetric maps intended to inform the deployment of instruments and the locations for the collection of sediment cores. The depth maps do not use a particular datum and are based on the depth during measurement, which was near high-tide. Thus, the depths should be considered approximate.

3.2. Hydrodynamic Data Acquisition and Processing

Frame-mounted oceanographic instruments were deployed at each of the five sites to measure hydrodynamic conditions near the bed over a 14-day neap-spring tidal cycle in November 2020 (Figure 1a). Frames were equipped with either a downward-looking Acoustic Doppler Current Profiler (ADCP; 2 MHz Nortek Aquadopp) operating in pulse-coherent mode to measure the time series of pressure and three components of velocity over a short near-bed profile (blanking distance of 0.05 and profile of 0.45 m) with 25-mm vertical resolution at 8-Hz temporal resolution, or an Acoustic Doppler Velocimeter (ADV; Nortek Vector), which measured pressure and velocities at a fixed point at 16 Hz. Data were recorded over a five-minute burst every 15 min. An optical backscatter sensor (Campbell Scientific OBS3+) was attached to each Nortek instrument to record turbidity at the same sampling rate as velocities. Two of the five sites (Sites 2 and 4) also had conductivity-temperature-depth sensors (CTD; RBR Concerto) coupled with Seapoint OBS sensors collecting measurements continuously at 6 Hz. OBS sensors were calibrated in the laboratory using bed sediment samples from the field site sieved through a 62.5 μm mesh to provide estimates of suspended sediment concentrations (SSC). A second-order polynomial fit forced through the origin provided a high-quality calibration (r^2 values between 0.91 and 1.00 for all instruments). Instrument deployment settings are summarized in Table S1 in Supporting Information S1.

For all pressure records, atmospheric variations were removed before conversion to water depth. Low correlation (<70%) velocity data from the pulse-coherent ADCPs were removed and gaps filled by linear interpolation (∼8.5% of in-water data), and corrected for phase wrapping (e.g., Lohrmann et al., 1990). ADV velocity data were similarly post-processed to remove low-quality data (correlations <70% or signal-to-noise ratios <15, <4% of data) and spikes (using the phase-space thresholding method of Goring and Nikora (2002)), with gaps filled by linear interpolation. Following quality control, velocity data were burst averaged and rotated into along-river (u, where $u > 0$ corresponds to seaward flow), across-river (v), and vertical (w) coordinates. RBR CTD data were averaged into 15-min bursts. The location of the riverbed (defined here as the sediment-water interface) was identified for each beam from the backscatter signal based on a critical threshold. The highest location identified across the three beams was selected to ensure no contamination from points below the interface in cases where the

instrument or bed orientation was not perfectly horizontal. Velocity data from below the identified interface were removed.

3.3. Surface Sediments and Sediment Cores

Surface sediment samples (upper ~5 cm) were collected in grids at each of the five study sites with a Ponar grab sampler. These grids consisted of five across-channel transects separated by 120–500 m. Within each transect, three to five samples were collected from the channel base. Following instrument retrieval, sediment cores (ranging from 0.91 to 2.76 m thick) were collected from the same locations (within ~10 m) as the oceanographic instrumentation using a tower-mounted vibracorer. Upon collection, the cores were stored upright at 6°C in a dark refrigerator. In the laboratory, cores were split in half, photographed, x-radiographed, logged, and sub-sampled for further analysis.

The grain size of surface sediment and core samples was analyzed using a Mastersizer 2000 laser particle size analyzer. Sediments were sieved through a 3.4 mm mesh, pre-treated with hydrogen peroxide, and agitated with sodium hexametaphosphate to deflocculate the clays. Gradistat software from Blott and Pye (2001) was used to statistically analyze grain size data to determine sediment classes and mean particle diameter using the Folk and Ward (1957) method.

A sub-set of sediments were dried at 60°C for 48 hr and then approximately 3 g was ground with a mortar and pestle. These samples were acidified using a 10% HCl solution, followed by multiple rinses with ultra-pure water. Acidified sediment was dried overnight at 60°C before being ground again for carbon stable isotope analyses of particulate organic matter ($^{13}C_{org}$).

Carbon-stable isotopes were analyzed with a DELTA V Plus continuous flow isotope ratio mass spectrometer linked to a Flash 2000 elemental analyzer using a MAS 200R autosampler (Thermo-Fisher Scientific, Bremen, Germany). Carbon isotope values are reported in per mille ‰, which is a measure of the deviation in the ratio of the measured ^{12}C–^{13}C from the Pee Dee Belemnite (PDB) standard. Enrichment in $^{13}C_{org}$ is calculated using the equation:

$$\delta^{13}C_{org}\ (‰) = (R_{sample} - R_{standard}) / (R_{standard}) \times 1000 \quad (1)$$

where, $R = {}^{13}C/{}^{12}C$.

3.4. Radiocarbon Dating and Age-Depth Modeling

Accelerator Mass Spectrometry (AMS) radiocarbon (^{14}C) analysis of bulk sediment organic matter was undertaken at the University of Waikato on selected sediment samples from cores. Sediment was washed in 1 M HCl at 80°C, followed by several hot 1 M NaOH washes. The NaOH insoluble fraction was reacidified with 1 M HCl at 80°C, filtered, rinsed with Milli-Q water to neutral, and dried at 80°C. The supernatant was removed after each step by pipette. CO_2 was collected by oxidation at 800°C overnight in the presence of pre-baked CuO and silver wire. The cryogenically separated CO_2 was then reduced to graphite with H_2 at 550°C using an iron catalyst (Stephenson). Pressed graphite was analyzed at the Keck Radiocarbon Dating Laboratory at the University of California Irvine on a NEC 0.5MV 1.5SDH-1 AMS system coupled with an in-house modified ion source (Beverly et al., 2010). All 14C ages were calibrated and converted to calendar years BP using OxCal v4.4.4 (Bronk Ramsey, 1995) with the SHCal20 curve (Hogg et al., 2020) and are reported at 95% probability.

The program rBacon was used for Bayesian age-depth modeling of sediment cores based on radiocarbon dates (Blaauw & Christen, 2011). This approach was used to constrain the geochronology by determining which parts of the stratigraphy are relevant to present-day hydrodynamic conditions and environments of deposition. Sediments that were modeled as younger than ~4,000 years old were considered relevant because this period is after the sea level and shoreline stabilized close to its present-day position (Figure S1 in Supporting Information S1) (Clement et al., 2016), and paleoenvironments in the area of the lower Waihou River would have been transitional fluvial-to-marine (Naish, 1990; Newnham et al., 1995).

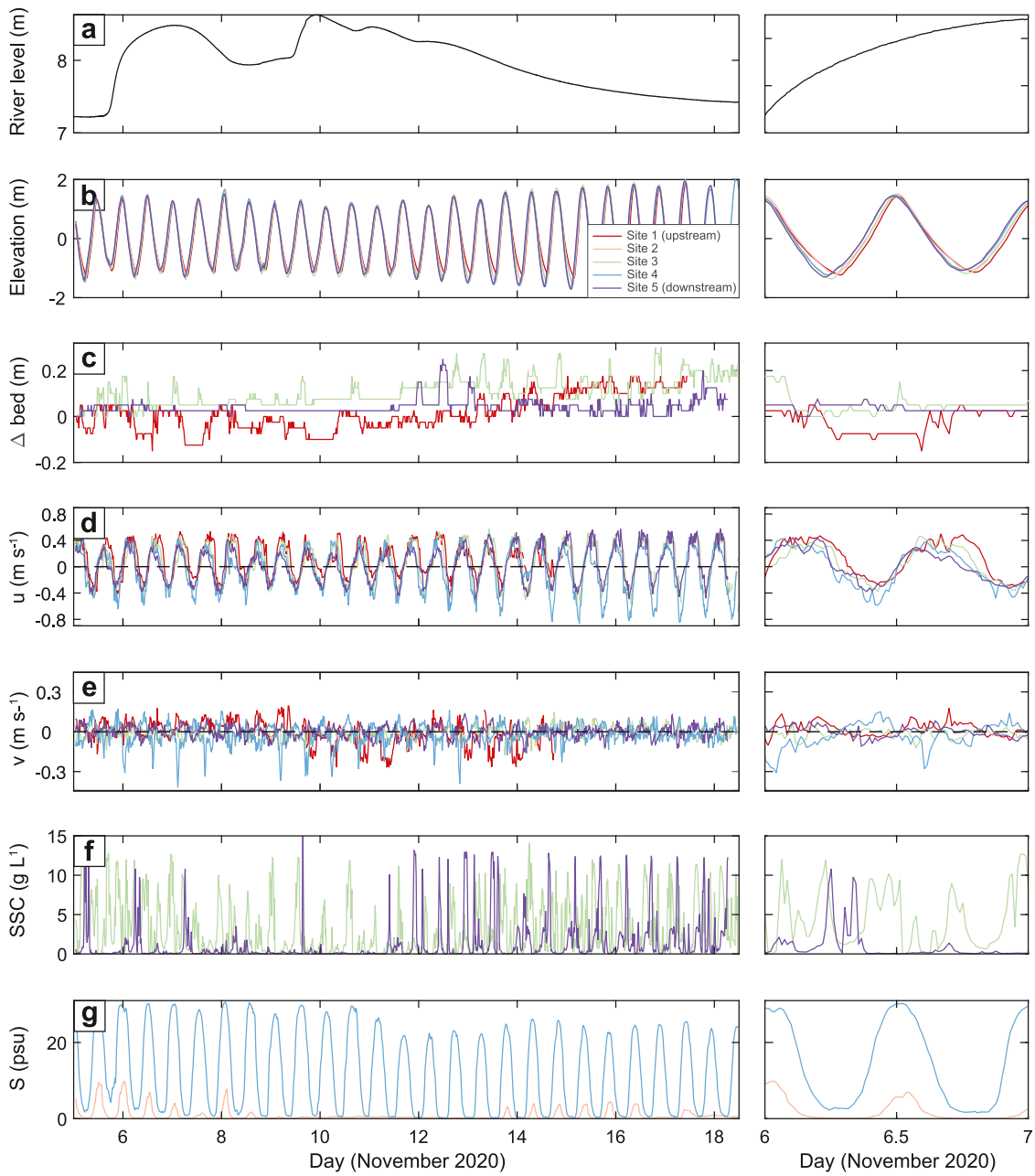

Figure 2 - two columns

Figure 2. Time series of hydrodynamic parameters for the full deployment (left column) and close-ups of one day (right column). (a) River level from Waikato Regional Council gauge located at Te Aroha (approximately 50 km upstream of Site 5). (b) Water surface elevation from Sites 1–5. (c) Change in bed elevation at Sites 1, 3, and 5. (d) Along-river velocities at Sites 1, 3, 4, and 5. (e) Across-river velocities at Sites 1, 3, 4, and 5. In (d), positive velocities correspond to seaward flow. (f) Suspended sediment concentrations at Sites 3 and 5. (g) Water salinity at Sites 2 and 4. In (d), (e), and (f), ADCP measurements are taken from the vertical bin at 0.1 m above the identified bed location (Figure S2 in Supporting Information S1).

4. Results and Interpretation

4.1. Hydrodynamic Processes

Near the start of instrument deployment (5th of November), water levels in the Waihou River increased abruptly over 12 hr from a baseline of ~7.2 m to reach ~8.3 m. Levels stayed above 8 m until peaking at 8.8 m on the 10th of November, after which water levels fell gradually to ~7.4 m (Figures 2a and 2b). Tidal amplitudes were similar

along the full stretch of the experimental section (Figures 2c and 2d) from ~2.2 m during neap tide to ~3.7 m during springs, with mean delays in high and low tide times between the river mouth (Site 5) and most upstream site (Site 1) of 24 and 89 min, respectively. There was more variability in delays in low tide times, indicating stronger river influences during the ebb phase of the tidal cycle. Measurements indicate that the maximum extent of saline water intrusion was likely somewhere between Sites 1 to 3 (i.e., ~6.3–13.7 river km): during the smallest tides at Site 2, the water column remained almost entirely fresh (<1 psu) throughout the tidal cycle (9–13th November), while the maximum salinity (9.8 psu) were reached on 6th of November for conditions with medium tidal amplitudes combined with lower river flows. In contrast, conditions at Site 4 varied between almost freshwater (0–4 psu) and (22–30 psu) marine over every tidal cycle (Figure 2h).

ADCP data indicate that near-bed current speeds along the river generally reached peak speeds of around 0.5 ms^{-1} at 0.1 m above the bed. Site 4 exhibited somewhat faster flow speeds of ~0.8 ms^{-1}, possibly owing to the measurement volume being positioned slightly higher in the water column. Unfortunately, the head of the ADV at Site 2 became buried/entangled, so no velocity data were available from this site. However, the current asymmetries changed with position along the river. Currents at Site 1 were strongly asymmetric and ebb-dominant with flood speeds about half of the ebb current speeds. Speeds dropped abruptly to close to 0 (<0.1 ms^{-1}) at both high and low tides. At the mid-river (Site 3), flows were much more tidally symmetric (with a slight ebb dominance). However, flows at Site 4 were flood-dominant throughout, while at the river mouth (Site 5) the dominance shifted over the deployment: during neap tides, flows were weakly flood-dominant, while during spring tides, flows were ebb-dominant. The duration of the high-water slack tide was the longest at Site 2, while the duration of the low-water slack tide was the longest at Site 5.

Bed elevations showed significant change at Sites 1 and 3 with net elevations increasing by ~0.25 m from the start of deployment and maximum sudden changes of ±0.15 (Site 1) and 0.2 m (Site 3) occurring over a few hours (Figure S2 in Supporting Information S1). Bed elevation was more stable at the river mouth corresponding to sandier conditions. Bed elevation variability at all sites was greater during spring tides.

Suspended sediment concentrations often exceeded the maximum instrument-resolvable values for the instruments Sites 1, 2, and 4 (inferred reliable values of ~3 g L^{-1}). Sites 3 and 5 had OBS sensors capable of resolving a larger turbidity range (calibrated up to ~18.6 g L^{-1}), so we predominantly focus on these two sites through the rest of the paper. At mid-river (Site 3), turbidity peaks were primarily associated with fast flow velocities at the bed (most commonly on the incoming tide) with multiple peaks above ~10 g L^{-1}. Several notable peaks developed at the end of the outgoing tide, reducing abruptly to ~0 at low water slack tides. At the river mouth, peaks in SSC (>10 g L^{-1}) typically occurred at the start of the flood tide and were often accompanied by a second peak at the end of the previous ebb (for spring tides). During the smaller tides and high river flows (November 8–11th) SSCs remained close to 0 g L^{-1} except a single peak on the afternoon of November 9th.

4.2. Sedimentology and Stratigraphy

4.2.1. Bathymetry and Surface Sediment Distribution

River width generally increases with distance downstream from 220 m upstream (Site 1) to 650 m at the river mouth (Site 5). Maximum depths in the vicinity of sampling sites were 6.5, 5, 5, 6.5, and 5.5 m at Sites 1 to 5, respectively (Figure 3).

The proportion of mud in surface sediments from channels displays a slight increase from upstream (Site 1) toward the mid-river position (Site 3), and then decreases toward the river mouth (Site 5) (Figure 3). The mean proportion of mud at Site 1 is 45% (range: 3%–99%, standard deviation: 42%), which increases to 48% at Site 2 (range: 5%–90%, standard deviation: 36%). Mud proportion increases further to 50% at Site 3 (range: 4%–97%, standard deviation: 39%), and from Site 3 seaward the mean proportion decreases. Site 4 has a mean proportion of 37% mud (range: 7%–86%, standard deviation: 28%), whereas Site 5 has the lowest mean proportion of mud at 35% (range: 4%–98%, standard deviation: 34%).

4.2.2. Radiocarbon Ages and Age-Depth Models

Twenty-six AMS radiocarbon dates of bulk sediment organic matter were obtained from the five cores. Radiocarbon ages ranged from 17,186 ± 46 BP (Core 2; 28–29 cm depth) to 448 ± 19 BP (Core 3; 26–27 cm depth)

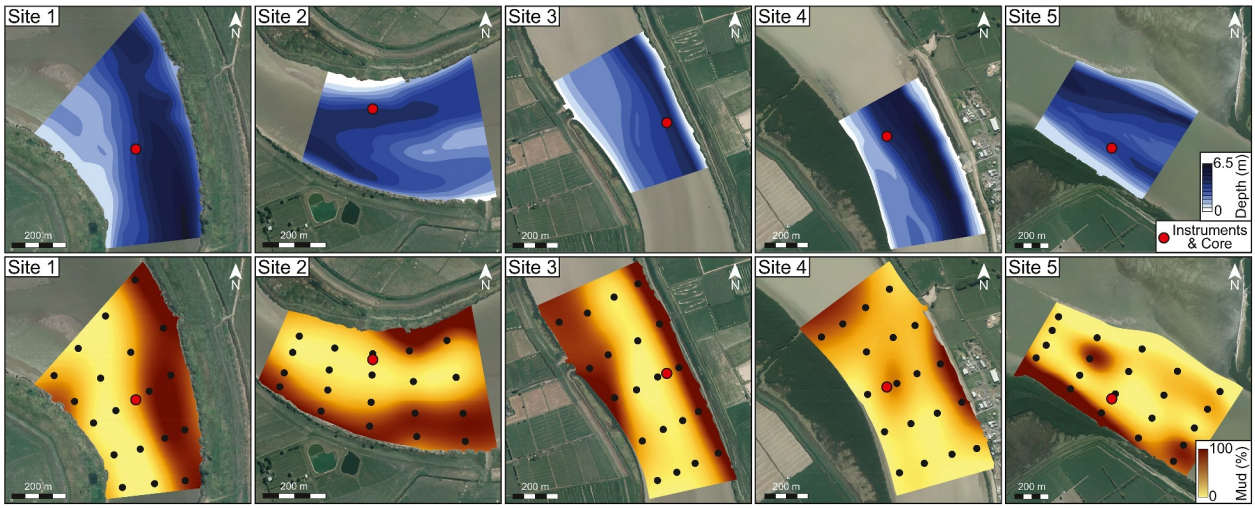

Figure 3. Maps showing the bathymetry (top row) and proportion of mud (<62.5 μm) in surface sediments (bottom row) for the five study sites. A red dot marks the precise co-location of instruments and sediment cores.

(Table S2 in Supporting Information S1). Four radiocarbon dates did not obey Walther's Law and were therefore rejected from age-depth modeling.

Age-depth models imply that Cores 1, 2, and 3 have a depositional break separating sediments older than ~8,300 to ~9,500 calendar years BP from much younger sediments ranging in age from ~960 to ~2,350 calendar years BP (Figure 4). This depositional hiatus represents a gap in time of between ~8,600 years (Core 1) and ~6,990 years (Core 2). The age-depth models also indicate that only the upper 28 cm in Core 1, 114 cm in Core 2, and 53 cm of Core 3 are likely to be relevant to the process-response linkages established herein.

4.2.3. Sedimentary Facies

The cored sedimentary successions at the five locations revealed eight recurring depositional units (i.e., facies): Facies A to Facies H (Figure 5; Table 1).

Facies A (FA) constitutes thin structureless mud laminae 2.5 mm thick with sharp basal and upper contacts (Figure 5a; Table 1). The mean grain size of Facies A is ~32 μm (coarse silt). This unit is deposited by gravitational settling from the water column during slack tide (Dalrymple et al., 2011; McCave, 1970).

Facies B (FB) comprises thick structureless mud laminae varying from 2.5 to 195 mm thick, with sharp basal contacts and gradational or deformed/loaded upper contacts (Figures 5a, 5b, and 5e; Table 1). Facies B has a mean grain size of ~12 μm (fine silt). These layers are fluid mud deposits frozen to the bed under unstable plug flow (Baas et al., 2009; MacKay & Dalrymple, 2011).

Facies C (FC) is composed of planar parallel laminated mud ranging from 9 to 50 mm thick, having sharp or gradational basal and upper contacts (Figures 5c–5e; Table 1). The mean grain size of Facies C is ~15 μm (fine silt). These units are rapidly deposited mud by unstable traction-dominated bedforms under quasi-steady transitional to plug flow conditions (Baas & Best, 2008; La Croix & Gingras, 2021; Lowe, 1988; MacKay & Dalrymple, 2011).

Facies D (FD; subdivided into D1 and D2) constitutes cross-laminated predominantly muddy laminae with sharp or gradational basal and upper contacts (Figures 5c–5e; Table 1). Facies D1 comprises muddy ripple lamination ranging in thickness from 5 to 75 mm with a mean grain size of ~25 μm (medium silt), while Facies D2 is composed of grain size gradational ripple lamination that varies between 7 and 12 mm thick with a grain size that varies from ~32 μm (coarse silt) to ~100 μm (very-fine sand). Laminae of Facies D represent traction transport and deposition of mud (D1) or mixed sand and mud (D2) under turbulent, transitional-turbulent, or transitional plug flow (Baas et al., 2009; La Croix & Gingras, 2021; MacKay & Dalrymple, 2011).

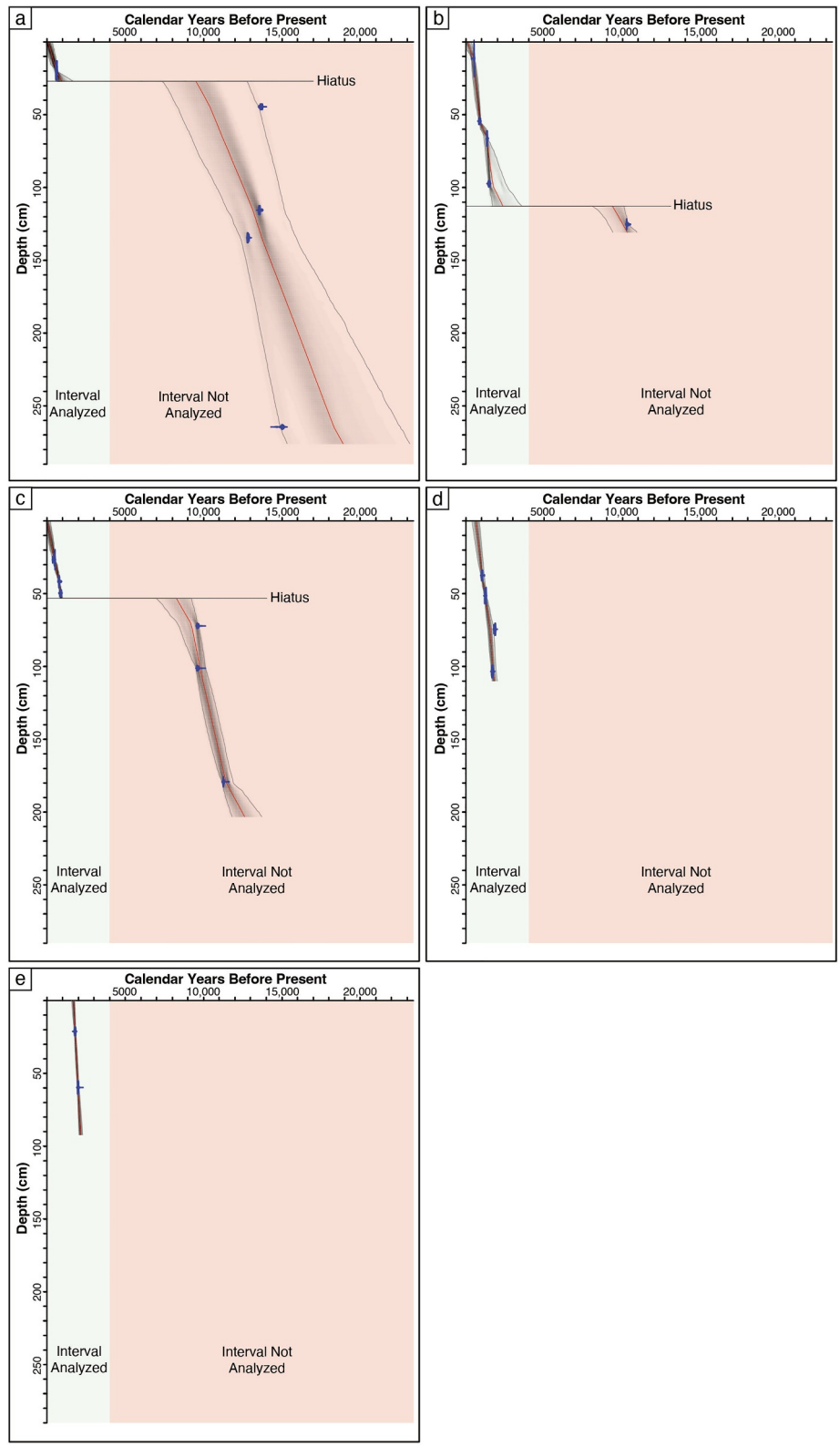

Figure 4. Bayesian age-depth models, constrained by radiocarbon dating of bulk organic carbon, for: (a) Core 1, (b) Core 2, (c) Core 3, (d) Core 4, and (e) Core 5. Note the presence of depositional hiatuses in Cores 1, 2, and 3, which are supported by sedimentologic and stratigraphic evidence. Models were built using rBacon (Blaauw & Christen, 2011).

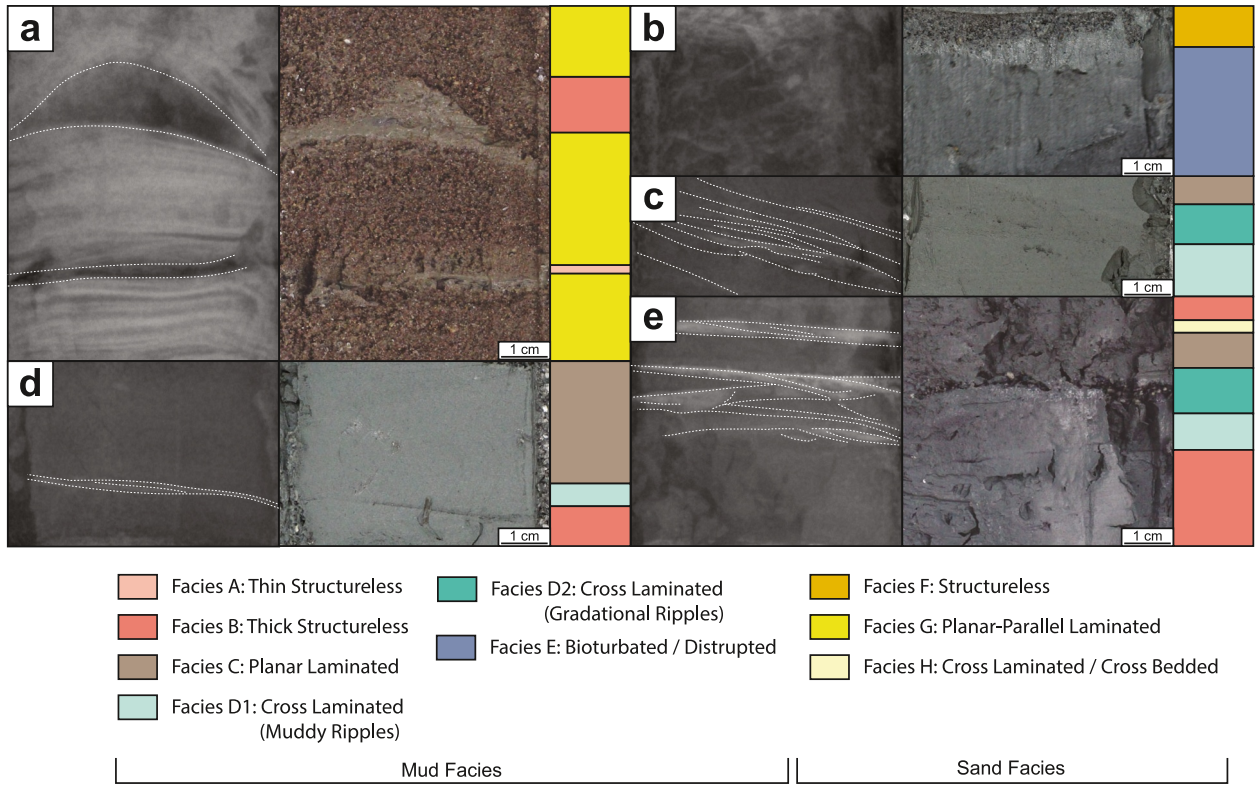

Figure 5. Examples of the eight recurring sedimentary facies observed in the cores. (a) Facies A, B, and G from Core 2, 3–12 cm depth. (b) Facies E and F from Core 3, 47–52 cm depth. (c) Facies C, D1, and D2 from Core 4, 95.5–99 cm depth. (d) Facies B, C, and D1 from Core 4, 63–68 cm depth. (e) Facies B, C, D1, D2, and H from Core 2, 84–90 cm depth.

Facies E (FE) is composed of bioturbated/disrupted mud with bioturbated or sharp basal and upper contacts, from 80 to 120 mm thick (Figure 5b; Table 1). The grain size of Facies E is variable ranging from ~15 μm (fine silt) to ~200 μm (fine sand). This facies displays post-depositional colonization of the substrate by infaunal organisms or salinity-tolerant plants and may have originally been any of the other mud-dominated facies (La Croix et al., 2015, 2022).

Facies F (FF) comprises structureless sand and muddy sand laminae/beds with sharp basal and upper contacts, which range in thickness from 35 to 420 mm (Figure 5b; Table 1). The mean grain size of Facies F is ~200 μm (fine sand). This facies is the product of rapid deceleration of sediment-laden flows (Martin & Turner, 1998; Shanmugam, 1997).

Facies G (FG) constitutes planar-parallel laminated sand laminae with sharp basal contacts and sharp or gradational upper contacts, ranging in thickness from 25 to 35 mm (Figure 5a; Table 1). Facies G has a mean grain size of ~240 μm (fine sand). These units result from traction transport and deposition by low-amplitude sand waves or along a planar depositional surface (Cheel, 1990).

Facies H (FH) consists of cross-laminated to cross-bedded sand with sharp or gradational basal and upper contacts (Figure 5e; Table 1). Facies H ranges in thickness from 25 to 165 mm and has a mean grain size of ~450 μm (medium sand). These laminae/beds form under turbulent flow and are the depositional expression of migrating ripples and dunes (Dalrymple & Choi, 2007).

4.2.4. Core Stratigraphy

Vibracores from along the FTT display a highly variable stratigraphy (Figure 6). Upstream in Core 1, the layering consists of 16.9 cm of FH, overlain by 1 cm of FD2, capped with 10.1 cm of FH. Further downstream in Core 2, the stratigraphy comprises 17 cm of interbedded FB and FH, overlain by 0.6 cm of FD2, and 10.8 cm of interbedded FC and FH. This succession is followed by 9.5 cm of interbedded FD1, FD2, and FB, passing upwards

Journal of Geophysical Research: Earth Surface

10.1029/2024JF007817

Table 1
Sedimentologic Characteristics of the Eight Recurring Sedimentary Facies, Along With Their Interpreted Mode of Formation

Facies	Thickness	Contacts	Mean grainsize	Depositional process
Muds				
Facies A: Thin Structureless	2.5 mm	Sharp basal; sharp upper	~32 μm (coarse silt)	Gravitational settling
Facies B: Thick Structureless	2.5–195 mm	Sharp basal; sharp, loading structures or gradational upper	~12 μm (fine silt)	Quasi-laminar plug or unstable plug flow
Facies C: Planar-Parallel Laminated	9–50 mm	Sharp or gradational basal; sharp or gradational upper	~15 μm (fine silt)	Transitional plug or quasi-laminar plug flow
Facies D1: Cross-Laminated (Muddy Ripples)	5–75 mm	Sharp or gradational basal; sharp or gradational upper	~25 μm (medium silt)	Turbulent, transitional-turbulent, or transitional-plug flow
Facies D2: Cross-Laminated (Gradational Ripples)	6–12 mm	Sharp or gradational basal; sharp or gradational upper	~32 μm (medium silt) to ~100 μm (very-fine sand)	Turbulent, transitional-turbulent, or transitional-plug flow
Facies E: Bioturbated/ Disrupted	8–120 mm	Bioturbated or sharp basal; bioturbated or sharp upper	Variable (~15–~200 μm; fine silt to fine sand)	Post-depositional colonization of substrate by infaunal organisms or salinity-tolerant plants
Sands				
Facies F: Structureless	35–410 mm	Sharp basal; sharp upper	~200 μm (fine sand)	Rapid deceleration of sediment-laden flows
Facies G: Planar-parallel Laminated	25–35 mm	Sharp basal; sharp or gradational upper	~240 μm (fine sand)	Upper flow regime traction transport-deposition by low-amplitude sand waves or along a planar depositional surface
Facies H: Cross-Laminated to Cross-Bedded	25–170 mm	Sharp or gradational basal; sharp or gradational upper	~450 μm (medium sand)	Lower regime turbulent flows. Migrating ripples and dunes

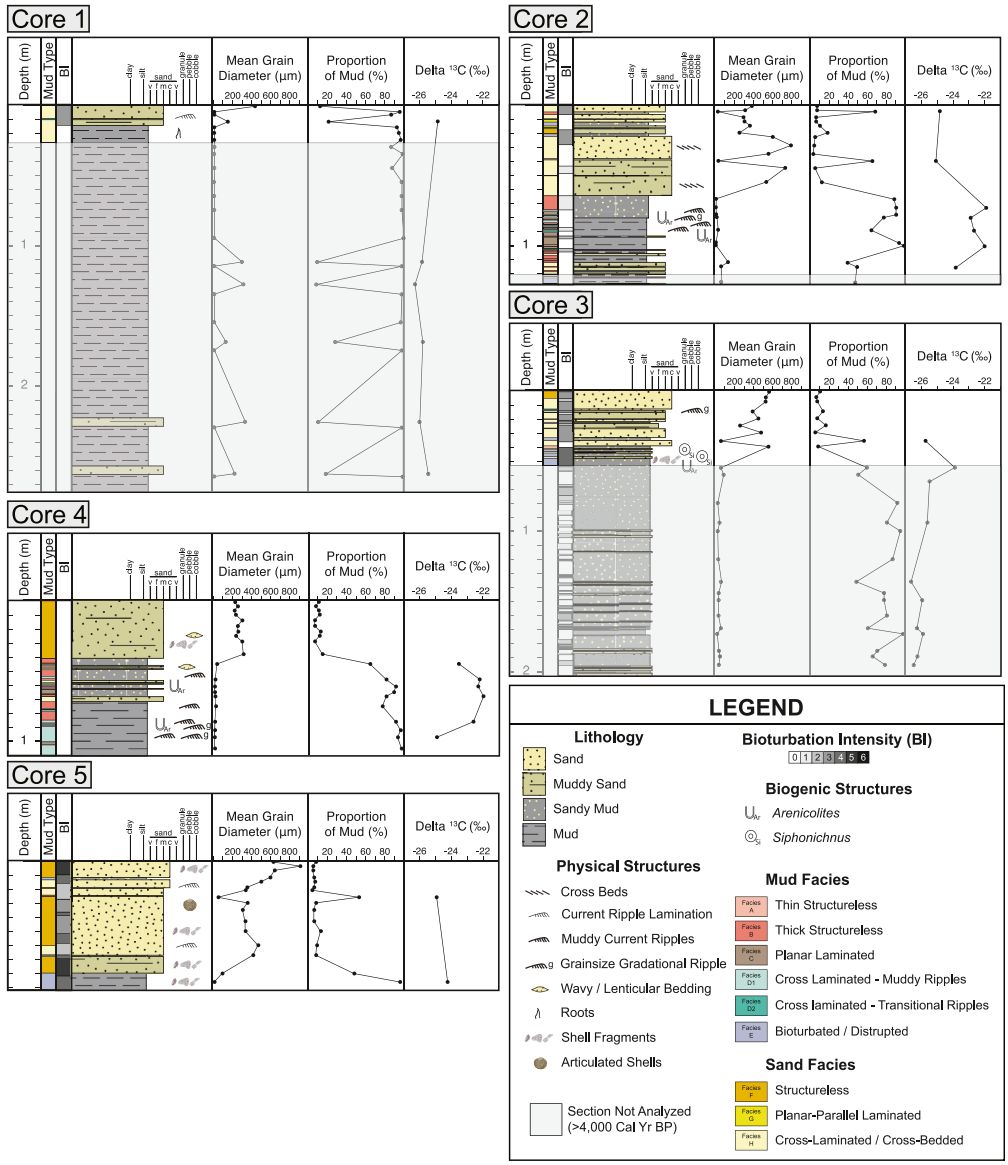

Figure 6. Core logs from vibracores collected along the Waihou River's FTT. The figure also displays the mean grain size, the proportion of mud (<62.5 μm), and $\delta^{13}C_{org}$ values determined from selected samples along the core profiles.

into 5.3 cm of FC and FD1. Atop this layer is 49 cm of FH with interspersed FA and FB, overlain by 11.2 cm of alternating beds of FE, FF, and FG. The succession is capped with 10 cm of interbedded FA, FB, and FH. Mid-river in Core 3, the stratigraphy constitutes 37.4 cm of interbedded FB, FE, and FH, overlain by 9.8 cm of interbedded FA, FD2, and FH, and capped with 5.8 cm of FF. Closer to the river mouth (Core 4), the stratigraphy is composed of 38.5 cm of interbedded FB and FD1, passing upwards into 16.3 cm of interbedded FB, FE, and FH, overlain by 14.3 cm of interbedded FB and FH, and capped with 40.9 cm of FF. Finally, at the river mouth in Core 5, the stratigraphy consists of 25 cm of interbedded FE and FF, overlain by 53.5 cm of FB, FF, and FH, passing into 1.6 cm of FE, capped with 12.1 cm of FF.

4.2.5. Carbon Stable Isotopes

Five surface samples and 16 core samples were analyzed for their $\delta^{13}C_{org}$ signatures, one sample from the surface at each site and several from the cored stratigraphic interval. $\delta^{13}C_{org}$ in surface sediments ranged from −22.82‰ (Site 1) to −24.94‰ (Site 4). Values in cores ranged from −22.03‰ (Core 4) to −24.3‰ (Core 2) (Table 2).

Table 2
$\delta^{13}C_{org}$ Measured in Bulk Mud Samples From Surface Sediments and the Five Sediment Cores

Location	Depth (cm)	$\delta^{13}C_{org}$ (‰)	Facies
Site 1	Surface	−22.82	N/A
Site 2	Surface	−24.42	N/A
Site 3	Surface	−23.82	N/A
Site 4	Surface	−24.94	N/A
Site 5	Surface	−23.19	N/A
Core 1	12	−24.87	Facies D1
Core 2	5	−24.8	Facies B
Core 2	40	−25.14	Facies C
Core 2	73	−21.97	Facies D1
Core 2	80	−22.95	Facies D1
Core 2	89	−22.74	Facies D2
Core 2	100	−22.07	Facies C
Core 3	36	−25.73	Facies E
Core 4	45	−23.58	Facies B
Core 4	56	−22.27	Facies B
Core 4	61	−22.36	Facies E
Core 4	68	−22.03	Facies B
Core 4	86	−22.66	Facies D1
Core 4	97	−24.96	Facies D2
Core 5	26	−24.96	Facies B
Core 5	86	−24.27	Facies E

Depleted (more negative) $\delta^{13}C_{org}$ values are taken to indicate increased terrestrial-sourced organic matter, whereas enriched (less negative) $\delta^{13}C_{org}$ values are taken to represent marine-sourced organic matter (Thornton & McManus, 1994).

5. Discussion

5.1. Static and Dynamic Process Regimes and Mud Deposits

Comparing the hydrodynamic process data (Figure 7a) with the mud regimes of Baas et al. (2009) as utilized by MacKay and Dalrymple (2011) allows us to estimate the different flow regimes present mid-river (Site 3) and at the river mouth (Site 5), which we infer provide the conditions necessary to deposit most of the mud-facies types observed in the core. Here, regimes are drawn from a direct first-order comparison using our measured data; the limitations of this approach are discussed in the next section. These regimes include: (a) an erosive-to-mud regime wherein only facies FG and FH are deposited, (b) a turbulent flow regime where facies FD1/FD2 and FH are stable, (c) a transitional turbulent flow regime where facies FD1/FD2 and FH are deposited, (d) a transitional plug flow regime within which facies FC and FD are stable, and (e) an unstable plug flow depositional regime in which facies FA and FB are deposited. Notably, we only recorded a single data point within the transitional plug flow regime and none within the quasi-laminar plug flow regime. We note that while the SSC values appear to be capped at around 10 g L^{-1}, this limit is much less than the maximum calibrated values for these instruments, and thus we conclude that the lack of values above ~10 g L^{-1} reflects the physical conditions and indicates the likely presence of fluid mud.

Our measurement of river-flow velocity and SSC suggest that the various flow regimes occurred for a different proportion of time during the field campaign (Figure 7b), and this proportion differed between the mid-river location (Site 3) and the river mouth (Site 5). At Site 3, turbulent flow dominated (51% of the time; Figure 7b), followed by transitional turbulent flow (20.2%), unstable plug flow/deposition (13.6%), and erosive-to-mud conditions (6.3%). For 4.6% of the time data was of low quality (i.e., low correlation factor), and 4.3% of the time the SSC fell below 0.01 g L^{-1}. Based on our interpretation at Site 5, turbulent flow also dominated (40.2% of the time) followed by erosive-to-mud conditions (26.6%), then unstable plug flow/deposition (24.5%), transitional turbulent flow (7.4%), and transitional plug flow (0.1%). SSC fell below 0.01 g L^{-1} 1.2% of the time.

Figures 7c–7f relates the flow regime conditions to tidal height in the channels. The start of the flood tide in the mid-river position is characterized by conditions that predominantly may reflect unstable plug flow and turbulent flow, and this transitions with rising tides to transitional turbulent flow, turbulent flow, and erosion-to-mud (Figure 7c). At the onset of the ebb tide, hydrodynamic conditions may shift from unstable plug flow/deposition to transitional turbulent flow, into turbulent flow, and finally erosion-to-mud (Figure 7d). During flood tide at the river mouth, hydrodynamic conditions are likely to begin in the unstable plug flow/deposition regime and with rising tide pass into transitional turbulent flow, turbulent flow, and eventually erosion-to-mud (Figure 7e). Finally, during the ebb tide, conditions may begin in the unstable plug flow/deposition regime, pass into the erosion-to-mud regime, and then into turbulent and transitional turbulent flows (Figure 7f).

Knowledge of the progression of hydrodynamic regimes with flood and ebb tides allows us to predict the progression of sedimentary facies that could theoretically be deposited during half-tidal cycles. Mid-river at Site 3, during the flood tide, we predict that continuous deposition resulting in a fully preserved sedimentary succession would consist of facies FA or FA + FB, passing upward into facies FD + FH, capped with facies FH (Figure 8a). During the ebb tide phase, facies FA would pass upward into facies FH, which would, in turn, be overlain by facies FD + FH (Figure 8b). At the river mouth at Site 5, the facies succession would comprise facies FA or FA + FB, passing upwards into facies FH (Figure 8c). During the ebb tide phase, facies FA would transition to facies FH (Figure 8d). However, these idealized sedimentary successions are not observed in any of the core

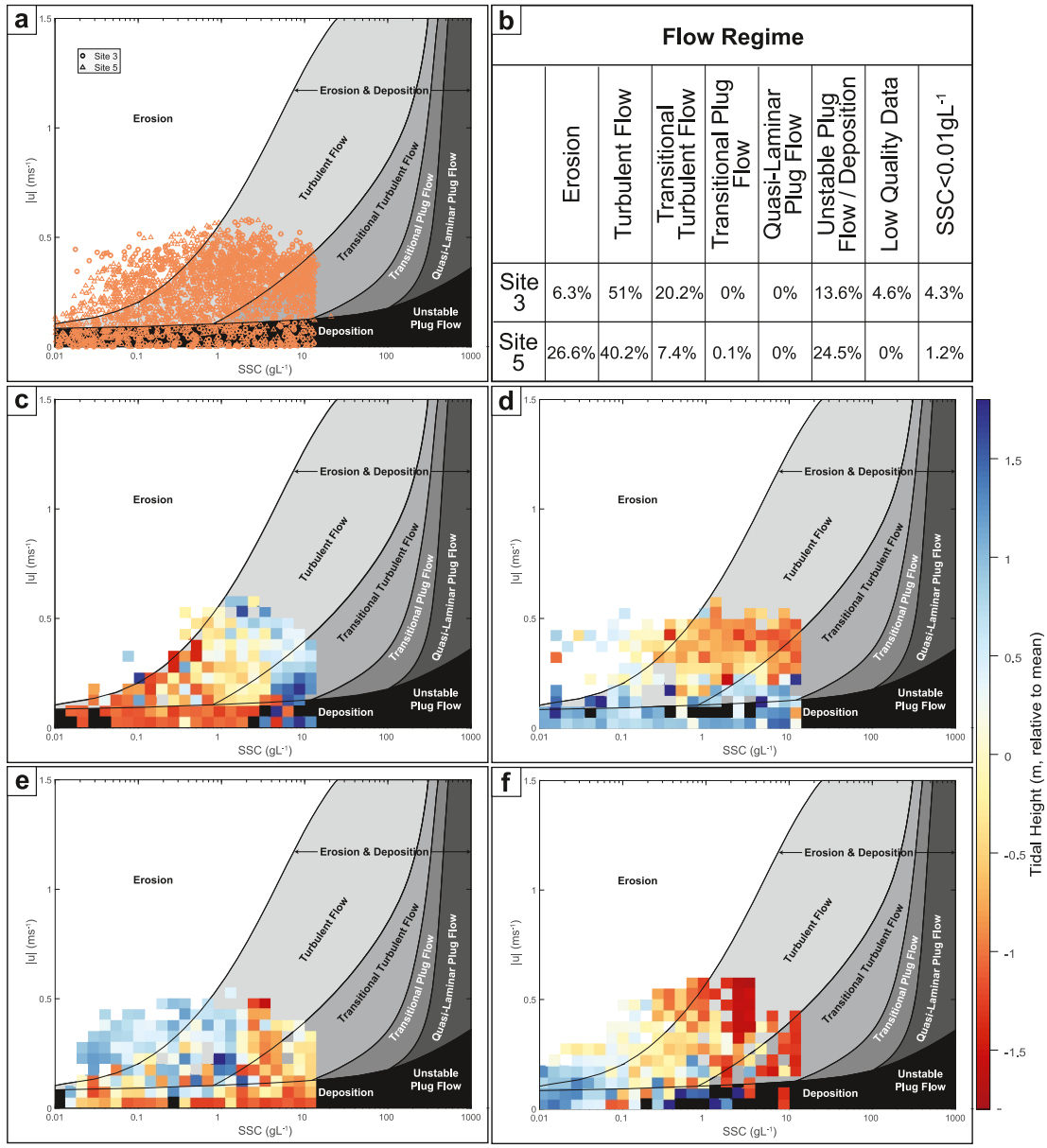

Figure 7. (a) Process observations from Sites 3 (mid-river) and 5 (river mouth) overlain on the flow regime diagram from MacKay and Dalrymple (2011) using the stability fields from Baas et al. (2009). While flow regimes from Baas et al. (2009) are depth-averaged, the present results are near-bed measurements. |u| is the horizontal flow speed 0.1 m above the bed and SSC is the suspended sediment concentration. (b) Proportion of the experimental duration in which hydrodynamic conditions fell into each flow regime. Average tidal height in relation to flow speed (|u|) and suspended sediment concentration (SSC) during flood (c) and ebb (d) tides at Site 3. (e) and (f) show the same as panels c and d for Site 5.

profiles (Figure 6), and this result suggests that the stratigraphy is fragmentary, with poor preservation potential of tidal cyclicity, possibly due to erosion of poorly consolidated or unconsolidated mud beds.

5.2. Hydrodynamic Uncertainty and Implications

Fluvial-estuarine settings are spatially and temporally complex from a hydrodynamic point of view. It has been well documented that velocity (Uncles & Stephens, 1990; Winterwerp et al., 2006), salinity (Kostaschuk & Atwood, 1990; Prandle, 1985), SSC (Kostaschuk et al., 1989), turbulence characteristics (Dejeans et al., 2022) and floc diameters (MacDonald & Mullarney, 2015) vary both horizontally and vertically through the water column over relatively short distances. Vertical velocity profiles in open channel flow often follow a logarithmic

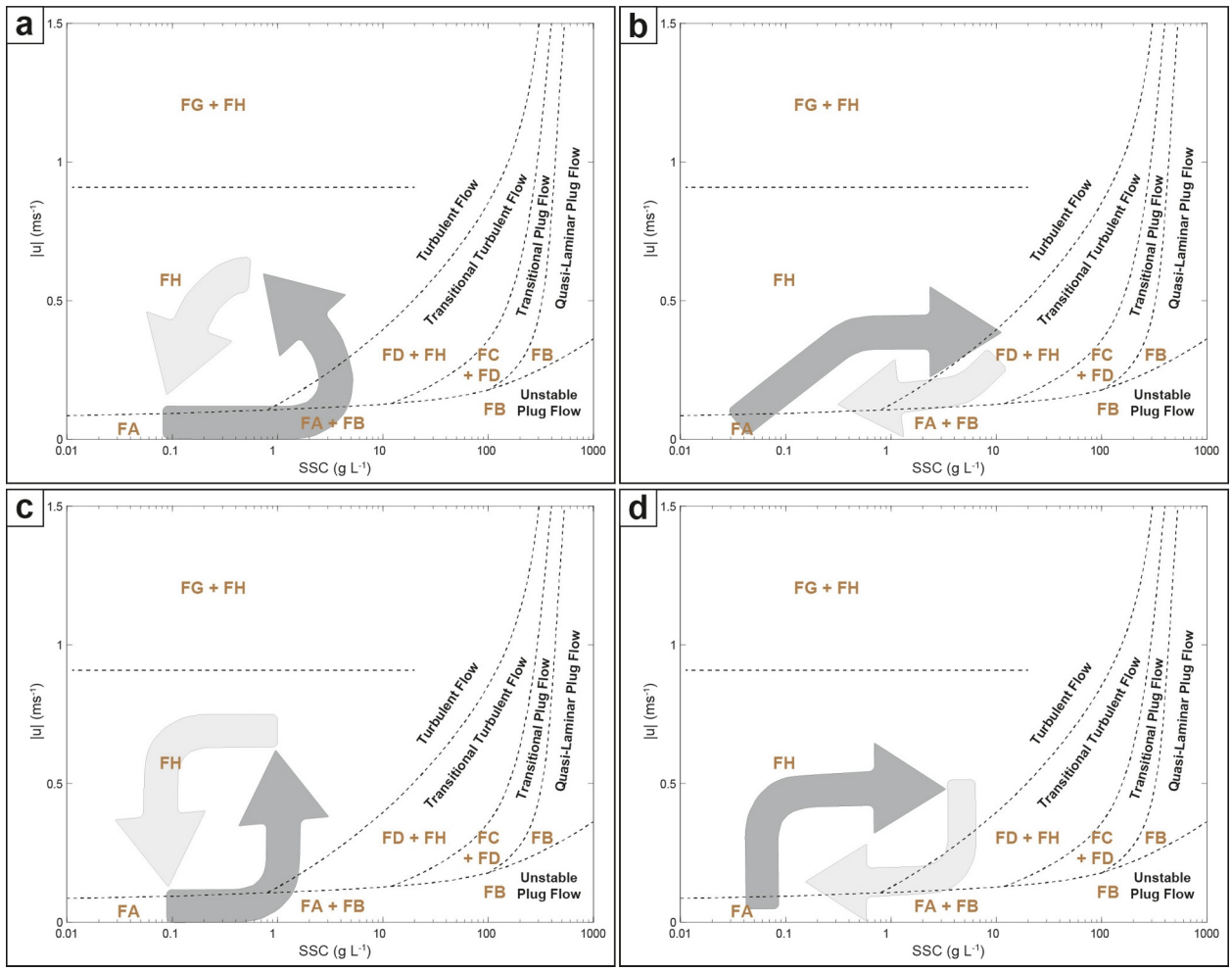

Figure 8. Flow stability diagrams displaying the suggested flow pathways and associated deposit types for: (a) Flood tide phase at Site 3 (mid-river); (b) Ebb tide phase at Site 3; (c) Flood tide phase at Site 5 (river mouth); and, (d) Ebb tide phase at Site 5. In the mid-river position, during the flood tide phase facies transition from FA or FA-FB to FD-FH, capped by FH. During the ebb tide phase facies transition from FA into FH, and then to FD + FH. By contrast, at the river mouth, during flood tides, the facies transition from FA or FA + FB to FH. During ebb tides, facies transition from FA to FH. The slack tidal period of time at both locations is so short (~15 min; Figure 3D) that no deposition occurs. Dark gray arrows show the progression of facies based on the quantitative flow regime data, whereas light gray arrows are conceptual indications of the rapid progression of conditions during the slack-tide.

relationship to distance from the bed (i.e., law of the wall; Van Rijn, 1990), while horizontal variations in flow velocities depend on the bathymetric profile and cross-sectional area of the river. Our measurement locations were selected to encompass the transition in the along-river direction from the almost entirely freshwater tidal regime to the marine tidal regime.

The flow regimes calculated by Baas et al. (2009) use depth-averaged flow velocity from an idealized flume experiment with fresh water, pure kaolinite, and a fixed, smooth, and flat bed. Moreover, their SSC profiles were very close to depth-uniform across all concentrations. We know that the lower Waihou River diverges from these idealized conditions in several ways, such as having variable bathymetry and bed roughness, changes in water salinity on tidal cycles, and a sediment load characterized by silt and clay particles composed of volcanic glass with some smectite (Naish et al., 1993). In addition, there are technical challenges in collecting profiles of velocity, SSC, and salinity in highly energetic and turbid waters such as the Waihou River. While we did not collect full water-profile measurements, recent data collected from the same stretch of river under similar river flow conditions to our experiment indicate that SSC values typically decrease sharply with height above the bed, with larger values (>1 g/L) only observed in the bottom 1-m of the water column (James, 2024). Thus, our SSC measurements are likely also greater than the depth-averaged values. However, for layered flow, without measurements of the vertical structure of velocities through the full water column, we cannot draw definitive

conclusions relating our measured speeds to depth-averaged values. It is plausible that our measurements would be approximately comparable to, but slower than, the average velocity in the lower layer of the water column. Hence, we restrict our interpretations of the graph as corresponding to processes in the lower layer only. This difference means that our data points would tend to sit further to the left on the abscissa and higher up the ordinate axes when transposed onto the regime diagram of MacKay and Dalrymple (2011); therefore, our interpretations linking point velocity and SSC to mud flow regimes should be treated as a first-order approximation. While the location of boundaries between regimes may vary, the general patterns of transitions between regimes likely still hold.

Additional differences between our study and the model of Baas et al. (2009) may include transitional flow behavior occurring at lower SSC due to the strong cohesive strength of smectite as well as the potential presence of extra polymeric substances in the bed sediments, which act to increase turbulence dampening at lower SSC. The extent of flocculation will also change along the river (owing to varying salinity and turbulence intensities), thus altering settling velocities; however, modeling results from a similar system indicate that conditions may be sufficiently energetic to prevent settling of even the larger flocs from the upper water column (Déjeans, 2023). Shifting topography at the bed and changes in bed roughness may also shift the boundaries between flow regimes to higher values due to increased turbulent mixing compared to Baas et al. (2009). Finally, the Waihou River transports a mixed sediment load, including organic material, of which the effects on flow regime conditions are unknown. However, despite these uncertainties, the signatures of the different regimes are nonetheless present in the sedimentary deposits. While we provide qualitative links between process and deposit, future research should focus on unraveling the myriad complexities of hydrodynamics and sedimentary deposits in natural fluvial–tidal systems to refine our understanding of these relationships.

5.3. Sedimentologic Trends Along the FTT

We analyzed the surface sediment and vibracore data to reveal longitudinal trends in the sedimentology of FTT of the Waihou River. The proportion of mud in surface sediments from channels displays a slight increase from upstream (Site 1) toward the mid-river (Site 3) and then river mouth (Site 5) (Figure 9a). This trend is linked to the process gradient as well as a decreasing supply of fine-grained sediment in the seaward direction. The locus of mud deposition occurs near the mid-river position, and this pattern is typical of deposits that accumulate near the time-average position of the turbidity maximum (La Croix & Dashtgard, 2014). However, there is wide variability in grain size at each site, which demonstrates significant variation in local-scale hydrodynamic conditions controlled by the highly variable flow speed and direction, changes in water salinity over short time scales, as well as differences in channel bed topography and roughness.

The trend in the proportion of mud in surface sediments along the FTT of the Waihou River is similar but less well-defined than other tidally influenced systems globally such as the Fraser River Delta (La Croix & Dashtgard, 2014), Mekong River Delta (Gugliotta et al., 2017), and Changjiang River Delta (Z. Wang et al., 2009). One major difference is that trends are compressed spatially in the Waihou River because of the short marine water inundation distance up the channel (~12 km) compared to lengths of ~30 km in the Fraser River Delta (Ages, 1979) or ~50 km in the Mekong River Delta (Gugliotta et al., 2017). The significant grain size variability at any location in the Waihou River is another point of contrast with these other large systems, but bears similarity to small FTTs such as the Kouchibouguac and Kouchibouguacis estuaries in Canada (Hauck et al., 2009). We interpret this difference to reflect complex movement of the turbidity maximum zone up and down the channel in response to the flashy river hydrograph, a reflection of the small drainage basin (see Mulder & Syvitski, 1995). This variability contrasts with the much larger drainage basins of the Fraser, Mekong, and Changjiang rivers, whose flow patterns are dictated by seasonal flow conditions rather than individual weather events (Gugliotta et al., 2017; La Croix et al., 2024; Z. Wang et al., 2009).

In addition to surface sediment characteristics, the stratigraphy of sediment cores also reveals trends in the overall proportion of sand and mud, as well as their facies characteristics (Figure 9b). Upstream in Core 1, sand dominates, constituting ~96% of the sediment (FH), with only ~4% mud (FD2). Downstream in Core 2, there is a more balanced composition of ~56% sand (3% FF, 2.6% FG, 49.4% FH) and ~44% mud (0.5% FA, 20.6% FB, 12% FC, 5.5% FD1, 1.5% FD2, 2.9% FE). Mid-river in Core 3, sedimentary layers are predominantly sandy, with ~69% sand (10.9% FF, 58.4% FH) and ~31% mud (1.1% FA, 3.4% FB, 1.8% FD2, 24.3% FE). Core 4 displays a lower proportion of sand, with ~45% sand (37.2% FF, 7.5% FH) and ~55% mud (25.9% FB, 5.9% FC, 22.2% FD1, 0.5% FD2, 0.7% FE). Finally, at the river mouth in Core 5,

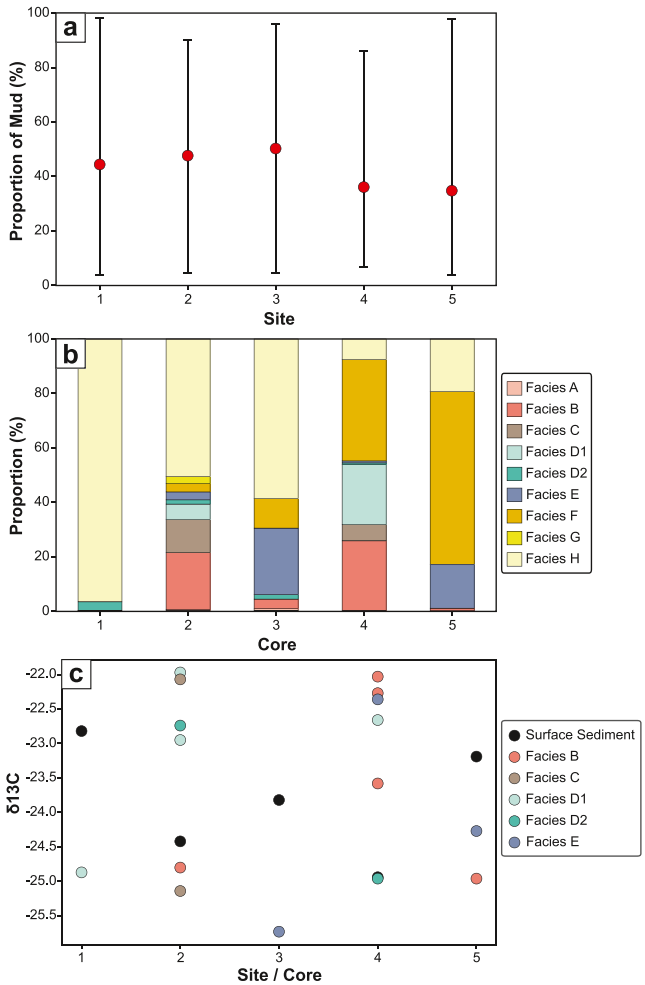

Figure 9. (a) Mean (red dot) and range in proportion of mud (<62.5 μm) in surface sediment samples. The plot shows a slight increase in the mean proportion of mud from Site 1 (upstream) toward Site 3 (mid-river), and then a decrease to Site 5 (river mouth). (b) Relative thickness-proportion of facies by core. All cores are dominated by sandy facies or show sub-equal proportions of sand and mud. Sites 2–4 show the greatest proportion and diversity of mud facies in their stratigraphic record. (c) $\delta^{13}C_{org}$ distribution for mud beds by site. The data suggest a mixture of terrestrial (more negative) and marine-sourced (less negative) values at all locations along the FTT of the Waihou River.

the stratigraphy is overwhelmingly sandy, comprising ~83% sand (63.8% FF, 19.2% FH) and ~17% mud (1.2% FB, 16% FE). Collectively, these stratigraphic patterns suggest that the time-averaged position of the turbidity maximum zone varied located approximately between Sites 2 and 4 through the last ~4,000 ka.

This study documents and quantifies the nature and distribution of mud facies through a modern FTT. Core analysis suggests that deposits from gravitational settling (i.e., "static mud" or FA) are relatively rare and/or rarely preserved in the stratigraphic record (Figures 6 and 9b). Facies FA only constitutes 0.5% of Core 2 and 1% of Core 3. On the other hand, "dynamic mud" is commonly observed and dominates the fine-grained sedimentary record. These dynamic mud deposits include so-called fluid muds (FB) and rapidly deposited mud from traction-dominated bedforms such as muddy ripples (FD1 and FD2). The results suggest that in small muddy tidally influenced rivers static mud deposition is the exception, whereas dynamic mud deposition is more typical.

While there is variation in $\delta^{13}C_{org}$ of mud deposits in surface sediments and cores, there is no clear trend relative to location or facies type (Figure 9c). All five locations within the FTT show indications of both terrestrial-sourced organic matter (more negative values) and marine-sourced organic matter (less negative values) (Thornton & McManus, 1994). In other words, it appears that the organic material being deposited alongside fine-grained sediments has a mixed terrestrial and marine source. However, we cannot discount the possibility that bank erosion is diluting this signature by progressively adding small amounts of terrestrial organic matter to flows downriver. This result differs from larger systems, such as the Fraser River Delta, where there is a progressive shift from terrestrial-sourced organic material toward marine-sourced organic material from the landward to the seaward end of the fluvial to marine transition (Czarnecki et al., 2014; Dashtgard et al., 2022). The observations from this study indicate that in small tidally influenced rivers, $\delta^{13}C_{org}$ is not a reliable proxy for longitudinal position in the channels owing to the complex mixing characteristics between marine and freshwater that occurs within a relatively narrow turbidity maximum zone.

5.4. Implications for the Rock Record

Understanding facies distribution in the FTT, and especially mud-prone facies, is essential for reconstructing past environments and sedimentary processes. Changes in mud distribution can reflect shifts in sediment dynamics or sea level changes affecting the position of the turbidity maximum zone, thus providing valuable information about the evolution of depositional conditions over time. However, although cyclic changes in river flow and marine-water intrusion up channels in the FTT are routinely interpreted from ancient strata (Collins et al., 2018; Gugliotta et al., 2016; Hovikowski et al., 2008; Jablonski & Dalrymple, 2016; La Croix et al., 2019; Lettley et al., 2007), these interpretations rely on observations of modern systems (e.g., Pearson & Gingras, 2006; Sisulak & Dashtgard, 2012), which may or may not be appropriate analogs to the strata to which the interpretations are applied.

When choosing an appropriate analog model, one must consider that the FTT of rivers with large drainage basins may be prone to preserving longer-term cyclicity (seasonal, annual) at the expense of short-term cycles (tidal, daily). This signal contrasts with small rivers with small drainage basins where the flood hydrograph may better resolve individual weather events and/or more subtle tidal cyclicity. An added complexity is the impact of climate on river flow patterns, with some regions subject to freeze-thaw (Hill et al., 2001), annual snowmelt-induced freshet (Dashtgard et al., 2012), or flashy monsoon-driven river flood cycles (Collins et al., 2018). The FTT of the Waihou River system does not record cyclic sedimentation patterns at any temporal or stratigraphic scale,

which is probably a function of the flashy nature of river flow. This study clearly shows that demonstrating cyclicity in the stratigraphic patterns is not a requirement for strata to be interpreted as having been deposited in the FTT. However, a combination of mixed-source organic matter as determined from $\delta^{13}C_{org}$, bioturbation by salinity-tolerant marine organisms, and dynamic mud deposits in the stratigraphic record could overcome the challenges of a lack of tidal-cycle preservation.

6. Conclusions

This study provides a detailed examination of hydrodynamic processes and sedimentary characteristics along the fluvial–tidal transition zone of the Waihou River, New Zealand. While previous studies have made linkages between deposits and processes in flume experiments under idealized conditions (e.g., Baas et al., 2009) or using the ancient record (e.g., MacKay & Dalrymple, 2011), here we explore a present-day sedimentary system. "Dynamic mud" hydrodynamic processes were recorded and linked at a first approximation with their associated deposits. Indeed, we interpret that the conditions necessary to deposit mud occurred during the full tidal cycle, including flood and ebb conditions. Through a large majority of the observation period, conditions were likely characterized by "dynamic mud" depositional regimes. In contrast, "static" mud conditions were only measured for a small proportion of the time. This dominance of "dynamic mud" conditions is also reflected in the mud beds preserved in the sediment cores.

The propensity to deposit different types of mud depends on location along the FTT. Overall, there is a downstream increase in the proportion of mud in surface sediments from landward to the mid-river, and then a slight decrease toward the river mouth. We attribute this trend to reflect the time-averaged position of the turbidity maximum zone. Carbon isotopes do not show a relationship to longitudinal position in the FTT or to facies type. This lack of pattern is likely owing to the complex hydrodynamic conditions and sedimentation patterns with both terrestrial and marine-sourced organic carbon. Similarly, cyclic deposition on daily, tidal, seasonal, or annual time scales was not observed in sediment cores. This omission is probably due to the flashy river hydrograph and temperate maritime climate. Thus, depositional cyclicity may not be a prerequisite for identifying FTT deposits in the ancient record. A combination of mixed-source organic matter, brackish-water trace fossils, and dynamic mud deposits can aid interpretation in the absence of cyclicity.

The implications of these findings extend beyond the Waihou River system and Aotearoa New Zealand. Understanding the hydrodynamic and sedimentary characteristics of the FTT from systems of all sizes and in diverse climatic regimes is essential for reconstructing past environments and interpreting sedimentary conditions from the geological past.

Data Availability Statement

Sedimentologic and hydrodynamic data used in this study can be accessed at La Croix et al. (2025).

Acknowledgments
We thank the University of Waikato field technician team (Warrick Powie, Chris Morcom, David Culliford, Alice Morrison) for their assistance with boats and diving. Brian and Sharon Coxhead of Bay Marine Works Ltd helped with barge-mounted coring. Radiocarbon analysis was undertaken at the Waikato Radiocarbon Laboratory. Carbon stable isotope analysis was undertaken at NIWA's Environmental and Ecological Stable Isotope Facility. Thank you Ngāti Maru and Russel Riki for blessing the field work and for Mātauranga Māori. The paper benefitted from feedback by three anonymous reviewers, Associate Editor Jaap Nienhuis, and Editor Ton Hoitink. This project was supported by a Strategic Research Grant from the University of Waikato. Open access publishing facilitated by The University of Waikato, as part of the Wiley - The University of Waikato agreement via the Council of Australian University Librarians.

References

Ages, A. (1979). The salinity intrusion in the Fraser River: Salinity, temperature and current observations 1976, 1977. In *Pacific Marine Science Report 79-14, Canadian Department of Fisheries and Oceans* (p. 191). Institute of Ocean Sciences.

Armstrong, H., & Brasier, M. (2005). *Microfossils* (2nd ed.). Blackwell Publishing.

Baas, J. H., & Best, J. L. (2008). The dynamics of turbulent, transitional and laminar clay-laden flow over a fixed current ripple. *Sedimentology*, *55*(3), 635–666. https://doi.org/10.1111/j.1365-3091.2007.00916.x

Baas, J. H., Best, J. L., Peakall, J., & Wang, M. (2009). A phase diagram for turbulent, transitional, and laminar clay suspension flows. *Journal of Sedimentary Research*, *79*(4), 162–183. https://doi.org/10.2110/jsr.2009.025

Beverly, R. K., Beaumont, W., Tauz, D., Ormsby, K. M., von Reden, K. F., Santos, G. M., & Southon, J. R. (2010). The keck carbon cycle AMS laboratory, University of California, Irvine: Status report. *Radiocarbon*, *52*(2), 301–309. https://doi.org/10.1017/S0033822200045343

Blaauw, M., & Christen, J. A. (2011). Flexible paleoclimate age-depth models using an autoregressive gamma process. *Bayesian Analysis*, *6*(3), 457–474. https://doi.org/10.1214/11-ba618

Blott, S. J., & Pye, K. (2001). GRADISTAT: A grain size distribution and statistics package for the analysis of unconsolidated sediments. *Earth Surface Processes and Landforms*, *26*(11), 1237–1248. https://doi.org/10.1002/esp.261

Bronk Ramsey, C. (1995). Radiocarbon calibration and analysis of stratigraphy: The OxCal program. *Radiocarbon*, *37*(2), 425–430. https://doi.org/10.1017/S0033822200030903

Carling, P. A., Chateau, C. C., Leckie, D. A., Langdon, C. T., Scaife, R. G., & Parsons, D. R. (2015). Sedimentology of a tidal point-bar within the fluvial–tidal transition: River Severn Estuary, UK. In P. J. Ashworth, J. L. Best, & D. R. Parsons (Eds.), *Fluvial-tidal sedimentology. Developments in sedimentology* (Vol. 68, pp. 149–192). Elsevier.

Cheel, R. J. (1990). Horizontal lamination and the sequence of bed phases and stratification under upper-flow-regime conditions. *Sedimentology*, *37*(3), 517–529. https://doi.org/10.1111/j.1365-3091.1990.tb00151.x

Choi, K. S., Dalrymple, R. W., Chun, S. S., & Kim, S.-P. (2004). Sedimentology of modern, inclined heterolithic stratification (IHS) in the macrotidal Han River Delta, Korea. *Journal of Sedimentary Research*, *74*(5), 677–689. https://doi.org/10.1306/030804740677

Choi, K. S., Jo, J., & Kim, D. (2021). Tidal and seasonal controls on the stratigraphic architecture of blind tidal channel deposits in the fluvial-tidal transition of the macrotidal Sittaung River estuary, Myanmar. *Sedimentary Geology*, *426*, 106029. https://doi.org/10.1016/j.sedgeo.2021.106029

Clement, A. J. H., Whitehouse, P. L., & Sloss, C. R. (2016). An examination of spatial variability in the timing and magnitude of Holocene relative sea-level changes in the New Zealand archipelago. *Quaternary Science Reviews*, *131*, 73–101. https://doi.org/10.1016/j.quascirev.2015.09.025

Collins, D. S., Johnson, H. D., Allison, P. A., & Damit, A. R. (2018). Mixed process, humid-tropical, shoreline-shelf deposition and preservation: Middle Miocene-modern Baram Delta Province, Northwest Borneo. *Journal of Sedimentary Research*, *88*(4), 399–430. https://doi.org/10.2110/jsr.2018.19

Czarnecki, J. M., Dashtgard, S. E., Pospelova, V., Mathewes, R. W., & MacEachern, J. A. (2014). Palynology and geochemistry of channel-margin sediments across the tidal–fluvial transition, lower Fraser River, Canada: Implications for the rock record. *Marine and Petroleum Geology*, *51*, 152–166. https://doi.org/10.1016/j.marpetgeo.2013.12.008

Dalrymple, R. W., Baker, E. K., Harris, P. T., & Hughes, M. G. (2003). Sedimentology and stratigraphy of a tide-dominated, foreland-basin delta (Fly River, Papua New Guinea). In F. H. Sidi, D. Nummedal, P. Imbert, H. Darman, & H. W. Posamentier (Eds.), *Tropical deltas of Southeast Asia—sedimentology, stratigraphy, and petroleum geology* (Vol. 76, pp. 147–173). SEPM Society for Sedimentary Geology. https://doi.org/10.2110/pec.03.76.0147

Dalrymple, R. W., & Choi, K. S. (2007). Morphologic and facies trends through the fluvial-marine transition in tide-dominated depositional systems: A schematic framework for environmental and sequence-stratigraphic interpretation. *Earth-Science Reviews*, *81*(3–4), 135–174. https://doi.org/10.1016/j.earscirev.2006.10.002

Dalrymple, R. W., MacKay, D. A., Ichaso, A. A., & Choi, K. S. (2011). Processes, morphodynamics, and facies of tide-dominated estuaries. In R. A. J. Davis & R. W. Dalrymple (Eds.), *Principles of tidal sedimentology* (pp. 79–108). Springer.

Dashtgard, S. E., & La Croix, A. D. (2015). Sedimentological trends across the tidal–fluvial transition, Fraser River, Canada. In P. J. Ashworth, J. L. Best, & D. R. Parsons (Eds.), *Fluvial-tidal sedimentology. Developments in sedimentology* (Vol. 68, pp. 111–126). Elsevier. https://doi.org/10.1016/b978-0-444-63529-7.00005-5

Dashtgard, S. E., Venditti, J. G., Hill, P. R., Sisulak, C. F., Johnson, S. M., & La Croix, A. D. (2012). Sedimentation across the tidal-fluvial transition in the lower Fraser River, Canada. *The Sedimentary Record*, *10*(4), 4–9. https://doi.org/10.2110/sedred.2012.4

Dashtgard, S. E., Wang, A., Pospelova, V., Wang, P.-L., La Croix, A., & Ayranci, K. (2022). Salinity indicators in sediment through the fluvial-to-marine transition (Fraser River, Canada). *Scientific Reports*, *12*(1), 14303. https://doi.org/10.1038/s41598-022-18466-4

Déjeans, B. S. (2023). *Lagrangian observations and numerical modelling of hydrodynamics, turbulence, and sediment transport in a tidal river* (Ph.D. thesis) (p. 140). School of Science, University of Waikato.

Déjeans, B. S., Mullarney, J. C., & MacDonald, I. T. (2022). Lagrangian observations and modelling of turbulence along a tidally influenced river. *Water Resources Research*, *58*, e2020WR027894. https://doi.org/10.1029/2020WR027894

Fagherazzi, S., Edmonds, D. A., Nardin, W., Leonardi, N., Canestrelli, A., Falcini, F., et al. (2015). Dynamics of river mouth deposits. *Reviews of Geophysics*, *53*(3), 642–672. https://doi.org/10.1002/2014RG000451

Folk, R. L., & Ward, W. C. (1957). Brazos River bar: A study in the significance of grain size parameters. *Journal of Sedimentary Petrology*, *27*(1), 3–26. https://doi.org/10.1306/74d70646-2b21-11d7-8648000102c1865d

Goring, D. G., & Nikora, V. I. (2002). Despiking acoustic doppler velocimeter data. *Journal of Hydraulic Engineering*, *128*(1), 117–126. https://doi.org/10.1061/(ASCE)0733-9429(2002)128:1(117)

Griffiths, G. A., & Glasby, G. P. (1985). Input of river-derived sediment to the New Zealand continental shelf: I. Mass. *Estuarine, Coastal and Shelf Science*, *21*(6), 773–787. https://doi.org/10.1016/0272-7714(85)90072-1

Gugliotta, M., Flint, S. S., Hodgson, D. M., & Veiga, G. D. (2016). Recognition criteria, characteristics and implications of the fluvial to marine transition zone in ancient deltaic deposits (Lajas Formation, Argentina). *Sedimentology*, *63*(7), 1971–2001. https://doi.org/10.1111/sed.12291

Gugliotta, M., & Saito, Y. (2019). Matching trends in channel width, sinuosity, and depth along the fluvial to marine transition zone of tide-dominated river deltas: The need for a revision of depositional and hydraulic models. *Earth-Science Reviews*, *191*, 93–113. https://doi.org/10.1016/j.earscirev.2019.02.002

Gugliotta, M., Saito, Y., Nguyen, V. L., Ta, T. K. O., Nakashima, R., Tamura, T., et al. (2017). Process regime, salinity, morphological, and sedimentary trends along the fluvial to marine transition zone of the mixed-energy Mekong River delta, Vietnam. *Continental Shelf Research*, *147*, 7–26. https://doi.org/10.1016/j.csr.2017.03.001

Hadfield, J. (2001). Waikato. In M. R. Rosen & P. A. White (Eds.), *Groudwaters of New Zealand* (pp. 315–326). New Zealand Hydrological Society.

Hauck, T. E., Dashtgard, S. E., Pemberton, S. G., & Gingras, M. K. (2009). Brackish-water ichnological trends in a microtidal barrier island/embayment system, Kouchibouguac National Park, New Brunswick, Canada. *PALAIOS*, *24*(8), 478–496. https://doi.org/10.2110/palo.2008.p08-056r

Hicks, D. M., Shankar, U., McKerchar, A. I., Basher, L., Lynn, I., Page, M., & Jessen, M. (2011). Suspended sediment yields from New Zealand rivers. *Journal of Hydrology*, *50*(1), 81–142.

Hill, P. R., Lewis, C. P., Desmarais, S., Kauppaymuthoo, V., & Rais, H. (2001). The Mackenzie delta: Sedimentary processes and facies of a high-latitude, fine-grained delta. *Sedimentology*, *48*(5), 1047–1078. https://doi.org/10.1046/j.1365-3091.2001.00408.x

Hochstein, M., & Balance, P. (1993). Hauraki Rift: A young, active, intra-continental rift in a back-arc setting. In P. F. Balance & K. J. Hsu (Eds.), *Sedimentary basins of the world* (pp. 295–305). Elsevier.

Hogg, A. G., Heaton, T. J., Hua, Q., Palmer, J. G., Turney, C. S. M., Southon, J., et al. (2020). SHCal20 Southern Hemisphere calibration, 0–55,000 Years cal BP. *Radiocarbon*, *62*(4), 759–778. https://doi.org/10.1017/RDC.2020.59

Hoitink, A. J. F., & Jay, D. A. (2016). Tidal river dynamics: Implications for deltas. *Reviews of Geophysics*, *54*(1), 240–272. https://doi.org/10.1002/2015RG000507

Hovikowski, J., Räsänen, M., Gingras, M., Ranzi, A., & Melo, J. (2008). Tidal and seasonal controls in the formation of Late Miocene inclined heterolithic stratification deposits, western Amazonian foreland basin. *Sedimentology*, *55*(3), 499–530. https://doi.org/10.1111/j.1365-3091.2007.00907.x

Jablonski, B. V. J., & Dalrymple, R. W. (2016). Recognition of strong seasonality and climatic cyclicity in an ancient, fluvially dominated, tidally influenced point bar: Middle McMurray Formation, Lower Steepbank River, north-eastern Alberta, Canada. *Sedimentology*, *63*(3), 552–585. https://doi.org/10.1111/sed.12228

James, B. (2024). *Measurements and modelling of the tidal salt intrusion along the Waihou River* (M.Sc. (Research) thesis) (p. 116). School of Science, University of Waikato.

Jay, D. A., Talke, S. A., Hudson, A., & Twardowski, M. (2015). Estuarine turbidity maxima revisited: Instrumental approaches, remote sensing, modeling studies, and new directions. In P. J. Ashworth, J. L. Best, & D. R. Parsons (Eds.), *Fluvial-tidal sedimentology. Developments in sedimentology* (Vol. 68, pp. 49–126). Elsevier.

Keevil, C. E., Parsons, D. R., Keevil, G. M., & Ainsley, M. (2015). Three-dimensional meander bend flow within the tidally influenced fluvial zone. In P. J. Ashworth, J. L. Best, & D. R. Parsons (Eds.), *Fluvial-tidal sedimentology. Developments in sedimentology* (Vol. 68, pp. 127–148). Elsevier. https://doi.org/10.1016/b978-0-444-63529-7.00006-7

Kostaschuk, R. A. (2002). Flow and sediment dynamics in migrating salinity intrusions: Fraser river estuary, Canada. *Estuaries*, *25*(2), 197–203. https://doi.org/10.1007/Bf02691307

Kostaschuk, R. A., & Atwood, L. A. (1990). River discharge and tidal controls on salt-wedge position and implications for channel shoaling—Fraser-River, British-Columbia. *Canadian Journal of Civil Engineering*, *17*(3), 452–459. https://doi.org/10.1139/l90-049

Kostaschuk, R. A., Luternauer, J. L., & Church, M. A. (1989). Suspended sediment Hysteresis in a salt-wedge estuary—Fraser-River, Canada. *Marine Geology*, *87*(2–4), 273–285. https://doi.org/10.1016/0025-3227(89)90065-0

La Croix, A. D., Ayranci, K., & Dashtgard, S. E. (2022). Neoichnology of siliciclastic shallow-marine environments: Invertebrates, traces, and environmental conditions. *Earth-Science Reviews*, *233*, 104170. https://doi.org/10.1016/j.earscirev.2022.104170

La Croix, A. D., & Dashtgard, S. E. (2014). Of sand and mud: Sedimentological criteria for identifying the turbidity maximum zone in a tidally influenced river. *Sedimentology*, *61*(7), 1961–1981. https://doi.org/10.1111/sed.12126

La Croix, A. D., & Dashtgard, S. E. (2015). A synthesis of depositional trends in intertidal and upper subtidal sediments across the tidal–fluvial transition in the Fraser River, Canada. *Journal of Sedimentary Research*, *85*(6), 683–698. https://doi.org/10.2110/jsr.2015.47

La Croix, A. D., Dashtgard, S. E., Gingras, M. K., Hauck, T. E., & MacEachern, J. A. (2015). Bioturbation trends across the freshwater to brackish-water transition in rivers. *Palaeogeography, Palaeoclimatology, Palaeoecology*, *440*, 66–77. https://doi.org/10.1016/j.palaeo.2015.08.030

La Croix, A. D., Dashtgard, S. E., Hill, P. R., Ayranci, K., & Clague, J. J. (2024). The Holocene to modern Fraser River Delta, Canada: Geological history, processes, deposits, natural hazards, and coastal management. *Canadian Journal of Earth Sciences*, *61*(10), 1043–1075. https://doi.org/10.1139/cjes-2024-0041

La Croix, A. D., Dashtgard, S. E., & MacEachern, J. A. (2019). Using a modern analogue to interpret depositional position in ancient fluvial-tidal channels: Example from the McMurray Formation, Canada. *Geoscience Frontiers*, *10*(6), 2219–2238. https://doi.org/10.1016/j.gsf.2019.03.008

La Croix, A. D., & Gingras, M. K. (2021). Facies characteristics and stratigraphy of an Upper Cretaceous mud-dominated subaqueous delta: Medicine Hat Member (Niobrara Formation), Alberta, Canada. *Sedimentology*, *68*(6), 2820–2853. https://doi.org/10.1111/sed.12875

La Croix, A. D., Roche, B., & Mullarney, J. C. (2025). Sedimentologic and hydrodynamic data from the fluvial–tidal transition zone of the Waihou River, Aotearoa New Zealand [Dataset]. *Zenodo*. https://doi.org/10.5281/zenodo.14873501

Lettley, C. D., Pemberton, S. G., Gingras, M. K., Ranger, M. J., & Blakney, B. J. (2007). Integrating sedimentology and ichnology to shed light on the system dynamics and paleogeography of an ancient riverine estuary. In J. A. MacEachern, K. L. Bann, M. K. Gingras, & S. G. Pemberton (Eds.), *Applied ichnology*, *Short Course notes* (Vol. 52, pp. 147–166). SEPM (Society for Sedimentary Geology). https://doi.org/10.2110/pec.07.52.0147

Lohrmann, A., Hackett, B., & Røed, L. P. (1990). High resolution measurements of turbulence, velocity and stress using a pulse-to-pulse coherent sonar. *Journalf of Atmosphere and Ocean Technology*, *7*, 19–37. https://doi.org/10.1175/1520-0426(1990)007<0019:HRMOTV>2.0.CO;2

Lowe, D. R. (1988). Suspended-load fallout rate as an independent variable in the analysis of current structures. *Sedimentology*, *35*(5), 765–776. https://doi.org/10.1111/j.1365-3091.1988.tb01250.x

MacDonald, I. T., & Mullarney, J. C. (2015). A novel "FlocDrifter" platform for observing flocculation and turbulence processes in a Lagrangian frame of reference. *Journal of Atmospheric and Oceanic Technology*, *32*(3), 547–561. https://doi.org/10.1175/JTECH-D-14-00106.1

MacKay, D. A., & Dalrymple, R. W. (2011). Dynamic mud deposition in a tidal environment: The record of fluid-mud deposition in the Cretaceous Bluesky Formation, Alberta, Canada. *Journal of Sedimentary Research*, *81*(12), 901–920. https://doi.org/10.2110/jsr.2011.74

Maggi, F. (2009). Biological flocculation of suspended particles in nutrient-rich aqueous ecosystems. *Journal of Hydrology*, *376*(1–2), 116–125. https://doi.org/10.1016/j.jhydrol.2009.07.040

Martin, C. A. L., & Turner, B. R. (1998). Origins of massive-type sandstones in braided river systems. *Earth-Science Reviews*, *44*(1–2), 15–38. https://doi.org/10.1016/S0012-8252(98)00019-1

McBride, G., Reeve, G., Pritchard, M., Lundquist, C., Daigneault, A., Bell, R., et al. (2016). The Firth of Thames and Lower Waihou River, climate changes, impacts and implications (CCII) for New Zealand to 2100 (p. 50).

McCave, I. N. (1970). Deposition of fine-grained sediment from tidal currents. *Journal of Geophysical Research*, *75*(21), 4151–4159. https://doi.org/10.1029/jc075i021p04151

Mulder, T., & Syvitski, J. P. M. (1995). Turbidity currents Generated at river mouths during exceptional discharges to the world oceans. *The Journal of Geology*, *103*(3), 285–299. https://doi.org/10.1086/629747

Naish, T. R. (1990). *Late Holocene sedimentation and diagenesis in the Firth of Thames: Bentonites in the making* (p. 154). University of Waikato.

Naish, T. R., Nelson, C. S., & Hodder, A. P. W. (1993). Evolution of holocene sedimentary bentonite in a shallow-marine embayment, Firth-of-Thames, New Zealand. *Marine Geology*, *109*(3–4), 267–278. https://doi.org/10.1016/0025-3227(93)90065-4

Newnham, R. M., de Lange, P. J., & Lowe, D. J. (1995). Holocene vegetation, climate and history of a raised bog complex, northern New Zealand based on palynology, plant macrofossils and tephrochronology. *The Holocene*, *5*(3), 267–282. https://doi.org/10.1177/095968369500500302

Nittrouer, C. A., DeMaster, D. J., Kuehl, S. A., Figueiredo, A. G., Jr., Sternberg, R. W., Faria, L. E. C., et al. (2021). Amazon sediment transport and accumulation along the continuum of mixed fluvial and marine processes. *Annual Review of Marine Science*, *13*(1), 501–536. https://doi.org/10.1146/annurev-marine-010816-060457

Pearson, N. J., & Gingras, M. K. (2006). An ichnological and sedimentological facies model for muddy point-bar deposits. *Journal of Sedimentary Research*, *76*(5), 771–782. https://doi.org/10.2110/jsr.2006.070

Potter, P. E., Maynard, J. B., & Depetris, P. J. (2005). *Mud and mudstones: Introduction and overview* (p. 297). Springer.

Prandle, D. (1985). On salinity regimes and the vertical structure of residual flows in narrow tidal estuaries. *Estuarine, Coastal and Shelf Science*, *20*(5), 615–635. https://doi.org/10.1016/0272-7714(85)90111-8

Pritchard, M., Swales, A., & Green, M. (2015). Influence of buoyancy- and wind-coupling on sediment dispersal and deposition in the Firth of Thames, New Zealand. In *Australasian Coasts & Ports Conference 2015: 22nd Australasian Coastal and Ocean Engineering Conference and the 15th Australasian Port and Harbour Conference* (pp. 733–738). Engineers Australia and IPENZ.

Prokocki, E. W., Best, J. L., Ashworth, P. J., Sambrook Smith, G. H., Nicholas, A. P., Parsons, D. R., & Simpson, C. J. (2020). Alluvial architecture of mid-channel fluvial–tidal barforms: The mesotidal Lower Columbia River, Oregon/Washington, USA. *Sedimentology*, *67*(7), 3533–3566. https://doi.org/10.1111/sed.12754

Roche, B. (2022). *Sedimentologic and hydrodynamic trends along a modern fluvial to marine transition zone: Mud deposition in the Lower Waihou River, Aotearoa-New Zealand* (M.Sc. (Research) thesis) (p. 73). School of Science, University of Waikato.

Schieber, J., Southard, J., & Thaisen, K. (2007). Accretion of mudstone beds from migrating floccule ripples. *Science*, *318*(5857), 1760–1763. https://doi.org/10.1126/science.1147001

Schieber, J., & Southard, J. B. (2009). Bedload transport of mud by floccule ripples—Direct observation of ripple migration processes and their implications. *Geology*, *37*(6), 483–486. https://doi.org/10.1130/g25319a.1

Shanmugam, G. (1997). The Bouma Sequence and the turbidite mind set. *Earth-Science Reviews*, *42*(4), 201–229. https://doi.org/10.1016/S0012-8252(97)81858-2

Sisulak, C. F., & Dashtgard, S. F. (2012). Seasonal controls on the development and character of inclined heterolithic stratification in a tide-influenced, fluvially dominated channel: Fraser River, Canada. *Journal of Sedimentary Research*, *82*(3–4), 244–257. https://doi.org/10.2110/jsr.2012.21

Small, L. F., & Prahl, F. G. (2004). A particle conveyor belt process in the Columbia River estuary: Evidence from chlorophylla and particulate organic carbon. *Estuaries*, *27*(6), 999–1013. https://doi.org/10.1007/BF02803426

Smith, D. G. (1987). Meandering river point bar lithofacies: Modern and ancient examples compared. In E. Etbridge, R. Flores, & M. Harvey (Eds.), *Recent developments in fluvial sedimentology* (pp. 83–91). SEPM, Special Publication No. 39.

Smith, D. G. (1988). Modern point bar deposits analogous to the Athabasca oil sands. In P. L. de Boer, A. van Gelder, & S. D. Nio (Eds.), *Tide-influenced sedimentary environments and facies* (pp. 417–432). Springer.

Sun, C.-C., Wang, Y.-S., Li, Q. P., Yue, W.-Z., Wang, Y.-T., Sun, F.-L., & Peng, Y.-L. (2012). Distribution characteristics of transparent exopolymer particles in the Pearl River estuary, China. *Journal of Geophysical Research*, *117*(G4). https://doi.org/10.1029/2012JG001951

Sutherland, B. R., Barrett, K. J., & Gingras, M. K. (2014). Clay settling in fresh and salt water. *Environmental Fluid Mechanics*, *15*(1), 147–160. https://doi.org/10.1007/s10652-014-9365-0

Thornton, S. F., & McManus, J. (1994). Application of organic carbon and nitrogen stable isotope and C/N ratios as source indicators of organic matter provenance in estuarine systems: Evidence from the Tay Estuary, Scotland. *Estuarine, Coastal and Shelf Science*, *38*(3), 219–233. https://doi.org/10.1006/ecss.1994.1015

Uncles, R. J., & Stephens, J. A. (1990). The structure of vertical current profiles in a macrotidal, partly-mixed estuary. *Estuaries*, *13*(4), 349–361. https://doi.org/10.2307/1351780

van de Lageweg, W. I., Braat, L., Parsons, D. R., & Kleinhans, M. G. (2018). Controls on mud distribution and architecture along the fluvial-to-marine transition. *Geology*, *46*(11), 971–974. https://doi.org/10.1130/g45504.1

Van den Berg, J. H., Boersma, J. R., & van Gelder, A. (2007). Diagnostic sedimentary structures of the fluvial-tidal transition zone—Evidence from deposits of the Rhine and Meuse. *Netherlands Journal of Geosciences*, *86*(3), 287–306. https://doi.org/10.1017/s0016774600077866

Van Rijn, L. C. (1990). *Principles of fluid flow and surface waves in rivers, estuaries, seas and oceans* (p. 335). Aqua Publications.

Vundavilli, H., Mullarney, J. C., MacDonald, I. T., & Bryan, K. R. (2021). The interaction of buoyant coastal river plumes with vegetation and consequences for sediment deposition and erosion in a tidal environment. *Continental Shelf Research*, *222*, 104417. https://doi.org/10.1016/j.csr.2021.104417

Wang, A., Wang, Z., Liu, J., Xu, N., & Li, H. (2021). The Sr/Ba ratio response to salinity in clastic sediments of the Yangtze River Delta. *Chemical Geology*, *559*, 119923. https://doi.org/10.1016/j.chemgeo.2020.119923

Wang, Z., Chen, Z., Li, M., Chen, J., & Zhao, Y. V. G. (2009). Variations in downstream grain-sizes to interpret sediment transport in the middle-lower Yangtze River, China, A pre-study of Three-Gorges Dam. *Geomorphology*, *113*(3–4), 217–229. https://doi.org/10.1016/j.geomorph.2009.03.009

Winterwerp, J. C., Wang, Z. B., van der Kaaij, T., Verelst, K., Bijlsma, A., Meersschaut, Y., & Sas, M. (2006). Flow velocity profiles in the Lower Scheldt estuary. *Ocean Dynamics*, *56*(3–4), 284–294. https://doi.org/10.1007/s10236-006-0063-4

Wu, H., Wang, Y. P., Gao, S., Xing, F., Tang, J., & Chen, D. (2022). Fluid mud dynamics in a tide-dominated estuary: A case study from the Yangtze River. *Continental Shelf Research*, *232*, 104623. https://doi.org/10.1016/j.csr.2021.104623